https://doi.org/10.15407/ufm.21.02.180

Yu.M. KOVAL[1], V.Z. KUTSOVA[2], M.A. KOVZEL[2], and P.Yu. SHVETS[2,*]

[1] G.V. Kurdyumov Institute for Metal Physics of the NAS of Ukraine,
36 Academician Vernadsky Blvd.,
UA-03142 Kyiv, Ukraine

[2] National Metallurgical Academy of Ukraine,
4 Gagarin Ave., UA-49000 Dnipro, Ukraine

* pavel22shvets@gmail.com

FEATURES OF STRUCTURE FORMATION, KINETICS OF PHASE TRANSFORMATIONS, MECHANICAL AND TRIBOLOGICAL PROPERTIES OF THE Fe-BASED Cr–Mn–Ni ALLOYS

The paper reviews and analyses solutions of theoretical and practical problem consisting in increasing the complex of tribological properties and heat resistance of the iron-based alloys for the state-of-the-art mechanical engineering industry. A composition of new sparingly alloyed wear-resistant iron-based chromium–manganese–nickel alloys is developed. The distribution of the alloying elements between phases and structural components is studied, the dependence of change of mechanical properties on structural parameters and phase composition is determined. For the first time, the kinetics of bainitic transformation and the regularities of forming a nanostructured bainitic matrix of Fe-based Cr–Mn–Ni alloys are investigated by means of dilatometric analysis. Diagrams of isothermal decomposition of supercooled austenite are plotted. Tribological properties of as-cast Cr–Mn–Ni alloys are studied.

Keywords: chromium–manganese–nickel alloys, structure, wear resistance, bainite, abrasive wear.

1. Introduction

Nowadays, increasing the service life of fast-wearing machine parts is a major problem in contemporary mechanical engineering (see, *e.g.*, review papers [1, 2] and references therein). Short service life of the parts

Citation: Yu.M. Koval, V.Z. Kutsova, M.A. Kovzel, and P.Yu. Shvets, Features of Structure Formation, Kinetics of Phase Transformations, Mechanical and Tribological Properties of the Fe-Based Cr–Mn–Ni Alloys, *Progress in Physics of Metals*, **21**, No. 2: 180–248 (2020)

reduces the cost efficiency of many machines and industrial equipment and results in permanent losses of metal. Solution of these challenges directly relates to improving properties of constructional materials including in particular sparingly alloyed high-chromium alloys.

Contemporary high-chromium alloys are complex alloyed multicomponent alloys of various structure and properties. They represent a separate group of industrial alloys: during solidification of these alloys, the carbide phase formed. In a combination with the determined type of matrix, this carbide phase determines specific properties of high-chromium alloys and at the same time, it causes significant difficulties during production and exploitation of these alloys.

High-chromium alloys have a complex metal matrix structure. Depending on the chemical composition, mass, cooling rate of the castings or the type of heat treatment, this matrix consists of austenite, martensite, and products of their decomposition. Correlation of these components can vary significantly.

One of the most efficient methods to improve operational characteristics of high-chromium alloys (cast irons) consists in a heat hardening. As known, the properties of cast iron castings can be significantly improved by heat treatment (to bainite in the solid state). However, currently the features of intermediate transformation of austenite in high-chromium alloys (with chromium content of 16–25%) are not widely covered in the current literature. At the same time, it should be noted that, despite the large number of works devoted to high-chromium cast irons, only a small number of works is devoted to the possibilities of heat treatment, phase and structural transformations, which are implemented in the solid state. The up-to-date literature also lacks data on the mechanism and features of intermediate transformation in sparingly doped high-chromium alloys with 16–25% of Cr. Data on the effect of composition and structure on operational properties of high-chromium cast irons are scarce.

Development of new heat hardening regimes (optimal for cast iron of this composition) requires careful experimental research of structure formation patterns, identification of relationships between the parameters of heat treatment and the structure formed, on the one hand, and characteristics of mechanical and service properties, on the other hand.

An experience of the (inter)national industry and special researches shows that high-chromium alloys containing 12–18% of chromium, 6–15% of manganese, and 0.8–1.2% of nickel are the most promising bearing materials for work in abrasive environments, impact loading conditions, and also in friction conditions at room temperature and elevated temperatures.

We arranged the present review paper as follows.

After the current (introduction) section, the next (second) one represents an overview of literary sources on the patterns of structure formation in high-chromium alloys and chromium–manganese–nickel alloys, contemporary ideas on the phase transformations of supercooled austenite in the solid state, which are implemented experimental alloys. Effects of alloying elements and heat treatment on the properties are considered as well.

The third section provides information on the data and techniques of our study. The objects of the research are samples of Cr–Mn–Ni alloys smelted in laboratory conditions with various levels of Cr, Ni, and Mn in the as-cast state and after heat treatment.

The fourth section investigates the structure, phase composition and properties of Cr–Mn–Ni alloys with Cr content of 12–16%, Mn content of 6–15%, and Ni content of 0.8–1.5% in the initial as-cast state, used for manufacturing parts of rolling tools of metallurgical equipment (rolling mills, rulers and rolling mill frameworks).

The fifth section deals with the regularities of bainitic-nanostructured-matrix formation in experimental Cr–Mn–Ni alloys.

The sixth section concerns the phase transformations of Cr–Mn–Ni alloys using a high-temperature differential thermal analyser. The liquidus and solidus temperatures are determined.

The seventh section represents influence of structural-phase state and stress-strain state, physicochemical and mechanical properties on tribotechnical characteristics of Cr–Mn–Ni alloys in the as-cast state. As determined, the maximum wear resistance and the minimum wear intensity are observed in chromium–manganese–nickel alloy with Cr content of 13%, Mn content of 15%, and Ni content of 1.2%.

Finally, the eighth section concludes and completes the work.

2. Contemporary Ideas about Structure Formation Patterns, Phase Composition, Mechanical and Tribological Properties of High-Chromium and Cr–Mn–Ni Alloys

2.1. Patterns of Structural Formation of Sparingly Alloyed High-Chromium Alloys

The most contemporary white wear-resistant cast irons are doped alloys. White unalloyed (plain) cast iron is used on a limited scale. Influence of alloying (doping) elements should be evaluated in connection with structure formation processes taking place during crystallization as well as in connection with the transformations occurring in the solid state.

Chromium is the main alloying element in the group of white wear-resistant cast irons being the most important in terms of importance and scope of application. Its content in this group of cast irons reaches the level of 35%. Chromium can partially replace iron atoms in or-

thorhombic iron carbide $(Fe,Cr)_3C$ or it can form chromium carbides where a certain part of chromium atoms is replaced by iron: trigonal one $(Cr,Fe)_7C_3$ and cubic one $(Cr,Fe)_{23}C_6$. In α-iron, chromium has unlimited solubility; while in γ-iron, it dissolves up to 12% Cr. Chromium carbides have significantly higher hardness in comparison with chromium-alloyed cementite, and this affects durability and strength of cast irons.

Nowadays high-chromium alloys doped with nickel and manganese are used as heat-resistant materials designed to be used at temperatures from T = 700 °C to 1100 °C. Due to their significant heat resistance, these alloys take one of the first places and are widely used in various fields of technology. This can be explained by the fact that heat-resistant alloys with high contents of manganese successfully combine high heat resistance, scale resistance (oxidation resistance) and adaptability to manufacture.

On the iron–carbon diagram, white cast irons are to the right of point E, meaning that they, unlike steels, must necessarily contain eutectic. Due to the large amount of cementite, these cast irons have a light breakage and therefore they are called as white.

In pre-eutectic white cast irons (<4.3% C), austenite is crystallized initially. It grows in the form of dendrites. During the initial crystallization of austenite, the liquid solution is enriched in carbon and, when its composition reaches point C, the eutectic $A + C$ (ledeburite) is crystallized. According to the lever rule, the ratio of austenite and cementite in ledeburite is 50/50.

Cementite is the basic phase initiating emergence of a cementite colony. On the cementite, plate formed in the eutectic fluid flat austenite dendrite grows. Subbranches of the basic cementite crystal grow between its branches. The pairwise (cooperative) growth of mutually intergrown crystals of the both phases takes place relatively quickly. Cementite is the leading phase in this pair growth. The specific nature of the pairwise growth of eutectic $A + C$ phases presupposes that the eutectic colony is gradually formed in the form of a cellular structure. In the cellular ledeburite, the basis (the colony matrix), is presented as a cementite crystal with rod-like branches of austenite crystal between its branches.

At high cooling rates, the austenitic-cement eutectic gets a lamellar, feathery structure instead of the cellular one. That is the result of splitting the leading phase, namely, cementite with austenite growing between its layers [3].

Ledeburite colonies are formed independently of initial austenite because its crystals are not the basic phase for formation of these colonies.

After consolidation is finished during cooling, the composition of austenite changes along the ES line and the secondary cementite is generated out of it. At slow cooling, all secondary cementite generated

from the initial and eutectic austenite, is layered onto the eutectic cementite and does not form an independent structural component. In case of accelerated cooling, the secondary cementite can be released as an independent structural component within large dendritic branches of the initial austenite, because in this case carbon does not have time to diffuse over relatively long distances to reach the initial austenite, namely, eutectic cementite.

When the secondary cementite is released, the composition of the austenite gets to the point *S* and, when supercooled below 727 °C, both initial austenite and eutectic austenite undergo eutectoid decomposition, becoming pearlite. Initial austenite dendrites retain their original outlines and therefore the respective structural component is referred to as transformed austenite.

Thus, at room temperature, you can see three structural components in pre-eutectic white cast iron, these components are (1) primary converted austenite, (2) secondary cementite (often undetectable), and (3) transformed ledeburite. White cast iron has high wear resistance under conditions of abrasive action, which can be attributed to the fact that carbon is in the form of solid compounds with metals (Fe, Cr, *etc.*), carbides and soft graphite are absent.

The structure of unalloyed and low-alloyed white cast iron consists of a pearlite matrix and carbides of Fe_3C or $(Fe,Cr)_3C$ types. It is less wear resistant in comparison with alloyed white cast iron (especially with the high-chromium one).

The wear resistance of low-alloyed white cast iron can be improved *via* adding small amounts of Ti, B, Cr, and Mn.

High-chromium wear-resistant cast iron is commonly smelted in electric arc furnaces or induction high frequency furnaces with acid or alkaline lining. The charge consists of processed low-silicon cast iron, its own return and ferroalloys. If a low-carbon ferrochromium is used, it is often necessary to carbonize additionally the metal with graphite debris. This cast iron intended for production of parts working in the abrasive wear conditions. Its most important feature is the ability to control durability and technological properties (machinability *via* cutting, casting properties) by means of selecting the appropriate chemical composition and heat treatment regime.

The structure of this cast iron is presented by special chromium carbide $(Cr,Fe)_7C_3$ and a metal base made of alloyed austenite or its decomposition products, depending on the cooling rate during casting and heat treatment. Good wear resistance under conditions of abrasive influence is provided by means of high carbide hardness (1300–1800 kg/mm^2) as well as *via* matrix strength.

Chromium presented in relatively small amounts in white cast iron (up to 5–8%) is a part of cementite type carbide $(Fe,Cr)_3C$ with an *HV*

microhardness of 950–1050 kg/mm^2. Special carbides $(Cr,Fe)_7C_3$ and $(Cr,Fe)_{23}C_6$ with microhardness of 1300–1800 kg/mm^2 are formed only in case of high chromium content. Minimal chromium contents necessary for formation of $(Cr,Fe)_7C_3$ carbides is approximately 10%.

White cast iron parts are intended for use under conditions of abrasive wear, and therefore high durability is the main requirement they must meet.

Alongside with low-alloyed chromium cast iron, high-alloyed chromium cast irons are also used in Ukrainian and international practice. The maximum operating temperature of low-alloyed cast iron (2.5% Cr) corresponds to 700 °C, and cast irons with a chromium content of 30–36% are recommended for temperatures of 1150–1200 °C.

Carbon content has a great influence on the structure and mechanical properties of chromium-alloyed cast irons. Chromium not only causes high heat resistance of cast irons, but also increases their wear resistance at elevated temperatures.

High-alloyed chromium cast irons have a somewhat weaker corrosion resistance in corrosive environments in comparison high-alloy low-carbon chromium steels, and that can be explained by presence of chromium carbides causing reduction of chromium content in the cast iron metal base. Chromium significantly increases corrosion resistance of cast irons.

Scale resistance (oxidation resistance) of high-alloyed chromium alloys in the air atmosphere does not practically change at increase of carbon content [3–5]. Wear resistance of a material is a characteristic of its ability to withstand wear and tear under certain conditions of external action [6]. Types of wear are diverse. They are determined by the variety of changes occurring in the contact layer during friction.

The physical and mechanical properties of the surface layer of the part being worn differ from the material properties in the volume of the workpiece due to surface phenomena associated with adsorption, oxidation *etc.* and determined by the intermediate environment, as well as due to stresses in the elastic and plastic area repeatedly occurring in the places of actual contact. These stresses and plastic deformation associated with them often lead to a profound change in the surface properties up to change in its chemical composition and phase composition [7, 8].

Wear occurring during friction of material that has come into chemical interaction with the environment is determined as corrosion-mechanical wear. In this case, destruction of the friction surface occurs in the issue of two simultaneous processes: corrosion and mechanical wear. Mechanical wear can then take place both during friction of the bonded surfaces and during interaction with the flow of the environment (liquid or gas, which may contain solid parts). In practice, one type of destruction of a worn surface can be rarely found, usually several types of

wear occur simultaneously, but one of these types is the leading one as for the rate of the process.

Thus, the properties of white cast irons with high contents of chromium combine high corrosion resistance and wear resistance in abrasive–corrosive environments with relatively high resistance in neutral environments due to expansion of the γ-region at manganese-alloying and appearance of bainitic-martensitic base structure after hardening. The variety of structural and chemical composition of cast irons makes it possible to vary significantly their operational properties.

2.2. Formation of the Structure of High-Chromium Alloys in the Bulky Castings

The article [9] presents results of investigation of microstructure of wear-resistant high chromium alloys (cast iron with chromium content of 15–18%) in bulky (massive) castings with a wall thickness of about 60 mm. It is recommended that cast iron be alloyed with nickel and molybdenum to provide a cast structure consisting of eutectic carbides, secondary dispersed carbides, bainite, martensite and austenite both unconverted and included in the bainite structure. Pearlite content in the structure must be 5%. Castings of such cast iron should be produced at temperatures of 450–550 °C. This microstructure provides a high durability of the cast iron under various operating conditions.

The studies were carried out using cast irons smelted in the laboratory and large castings of factory melts (with a Cr content of 16–18%). In laboratory conditions, high chromium alloys were melted in a Tamman furnace in a crucible with a capacity of up to 1.5 kg. In order to obtain a cast iron, microstructure typical for massive castings as a result of crystallization and phase transformations during slow cooling the cast iron was subjected to crystallization in the crucible with furnace off or partial heating applied. This regime of cast iron crystallization helped to obtain cast iron microstructure (size of dendrites and eutectic carbides) analogous to massive castings of cast irons produced in conditions of industrial smelting.

The microstructure of the austenite decomposition products of industrial smelting cast irons (with castings cooled in the form during a period of more than one day), was largely different from that of austenite decomposition products of cast irons obtained in the result of laboratory melting (with usually high cooling rate).

When developing the chemical composition of cast iron for massive castings, the problem is that the selected chemical composition after cast consolidation and its cooling should provide release of a minimum amount of dispersed carbides. At temperatures of eutectoid transformation, they (carbides) would not form a pearlite structure or would at

least form its minimal amount (less than 5%), and the bulk of austenite could undergo bainitic and martensitic transformation during further cooling. It should be noted that the final microstructure of a cast iron, where bainite and martensite are present, would always have austenite as a phase component of the bainite structure.

Such alloying elements as manganese, nickel, molybdenum, and copper are used to stabilize the austenite of chromium cast irons. X-ray diffraction analysis of cast iron structures with complicated identification of α- and γ-phase was performed in Ref. [10] using microscopes. However, the ratio of ferrite, α-phase of pearlite, α-phase of bainite and martensite (α-phase) was not investigated, but only the sum of these phase components was determined.

Microstructural analysis of high-chromium cast iron as the main method of study in metal science has made it possible to obtain the largest amount of information on the metal microstructure. Chemical analysis of the composition of the investigated cast irons, results of light microscopy and electron microscopy, x-ray diffraction analysis, microhardness of the phases, as well as accounting of published researches in this area gave an opportunity to determine microstructure formation peculiarities of these cast irons.

Concerning massive castings of wear-resistant high-chromium cast iron with a wall thickness of about 60 mm, it is recommended to use a cast iron containing 16–17% of Cr, alloyed with nickel and molybdenum (up to 1.5% of each component), of course, in each separate case, with workout adjustment of the cast iron chemical composition (in production conditions) primarily concerning the content of manganese, nickel and molybdenum. This adjustment gives an opportunity to obtain the microstructure of cast iron in a cast state without pearlite or with minimal content of pearlite.

Results of the investigation concerning formation of microstructures of high-chromium wear-resistant alloys (cast irons) enable to carry out more detailed and successful adjustment of technology for the production of massive castings (chromium wear-resistant cast irons).

2.3. Transformation of Austenite during Cooling in the Solid State

Distinctive features of transformations of supercooled cast iron austenite with $(Cr,Fe)_7C_3$ and $(Cr,Fe)_{23}C_6$ in comparison with low-chromium cast irons (with carbides of $(Fe,Cr)_3C$) are conditioned primarily by the fact that due to the high chromium content the γ-region is narrowed; additional molybdenum alloying also narrows the γ-region, and nickel or manganese alloying widens it. The limiting carbon concentration in austenite during chromium alloying is reduced significantly. The points *E* and *S* on the pseudobinary sections of the Fe–C–Cr diagram are shifted to higher temperatures.

Isothermal transformation of austenite in chromium cast irons of industrial grades with carbides $(Cr,Fe)_7C_3$ in the pearlite region is much faster than in case with Ni-hard type cast irons. This fact is determined by many reasons. The main of these reasons is the extremely active inhibition of pearlite transformation in Ni-hard cast iron by means of Ni, which is almost completely concentrated in the base, and significantly higher C content in austenite [11–15].

In the as-cast state, a significant amount of original austenite is usually retained in chromium cast irons. The stability of austenite during isothermal decomposition depends largely on how its composition has changed until the end of heating at the austenization temperature. During heating and soaking wear-resistant chromium cast irons for hardening two processes occur simultaneously: release of secondary carbides from supersaturated original austenite and $\alpha\rightarrow\gamma$-transformations at areas that were troostitic (pearlitic) after casting [16].

With the release of secondary carbides, austenite loses carbon according to the carbide solubility surface. Concentration of alloying elements (especially strong carbide-forming ones, primarily, chromium and molybdenum) also decreases. Secondary carbides are additional crystallization centres that facilitate pearlite decomposition at subcritical temperatures. Whether the equilibrium concentration of carbon and alloys corresponding to a given austenitization temperature is reached, it depends on the dynamics of the secondary carbide release from the supersaturated original austenite and the rates of diffusion equalization of the γ-phase composition at this temperature. The rate of release of secondary carbides in chromium wear-resistant cast irons has not been studied sufficiently [13].

Assessing impact of alloying elements on the transformation of austenite in wear-resistant cast irons, it is necessary to take into account the change of carbon concentration in it. This is because the austenite of a wear-resistant cast iron is always extremely saturated with carbon, and the solubility of carbon in the γ-phase strongly depends on the content of alloying elements (such as, *e.g.*, chromium). In its turn, the carbon content in austenite strongly affects the nature of transformations, especially the temperature of the martensitic transformation. Completeness of the martensitic transformation and stability of the residual austenite are the most important factors determining cast iron wear resistance.

Molybdenum is one of the most effective elements inhibiting decomposition of austenite in the pearlitic region and thereby dramatically increasing the hardening capacity [16]. The temperature of the martensitic transformation onset during molybdenum alloying of chromium cast iron is almost unchanged. Effect of molybdenum on the inhibition of pearlite transformation depends on the contents of carbon and chro-

mium in the cast iron. The minimum amount of molybdenum significantly affecting the position of the pearlite transformation region on thermokinetic diagrams is the smaller the greater the Cr/C ratio is. However, an increasing the molybdenum content over a certain limit does not lead to further intensive inhibition of pearlite decomposition. Service properties of cast irons with a higher Cr/C ratio and first of all their wear resistance are largely determined by a high initial temperature of the martensitic transformation.

Manganese alloying causes intensive reduction of martensitic transformation temperature. Therefore, during increasing manganese content, the fullness of martensitic transformation decreases simultaneously with the suppression of pearlite transformation (especially when the manganese content is >5%). As the manganese content in chromium cast iron is growing, the amount of residual austenite and its stability are increasing, and this affects its wear resistance.

Increased contents of carbon in wear-resistant cast iron lead to an increase of the amount of carbides. The decrease in the stability of austenite in the pearlite region with increase of carbon content in chrome–molybdenum cast iron can be explained by the decrease of chromium concentration in austenite. Increase of carbon concentration in γ-phase in this range of transformation plays a less important role. Decrease of the martensitic transformation temperature is determined by the carbon concentration increase, which obscures the effect of increasing this temperature due to the decrease of chromium concentration.

Silicon narrows the γ-region and raises critical points. As Si content in high-chromium cast iron reaches 2.5%, the AC3 point reaches 1200 °C, *i.e.*, it rises almost to the solidus level. Silicon limits the solubility of carbon in austenite and impedes its diffusion in γ-iron and α-iron [17, 18] Hardness of silicon-alloyed ferrite increases significantly. Fine-dispersed ferrite–carbide mixtures formed during decomposition of siliceous austenite are close to martensite in their hardness [19].

Investigations of influence (caused by the main alloying elements) of wear-resistant cast iron on the transformation of supercooled austenite in the pearlite and martensitic range showed that manganese, molybdenum, copper, chromium, and nickel inhibit the pearlite transformation, while carbon and silicon accelerate it. The initial temperature of martensitic transformation decreases with increasing amounts of silicon and chromium and does not depend on the molybdenum content within the studied frameworks [17].

2.4. Wear Resistance of High-Chromium and Sparingly Alloyed Cr–Mn–Ni

Wear of parts in the result of friction (which leads to loss of its operability) is the cause of premature failure of the most parts of machinery and equipment used in the sphere of metal industry, coal industry, industry of building materials, energy generating industry, *i.e.*, wherever mineral raw materials are processed, and there is a contact of the operating surface with abrasive parts. Wearing losses are estimated as thousands of tons of metal per year; and even greater damage is caused by decreased technological parameters of machines and mechanisms due to wear and tear of operating parts [20].

Wear of materials is the destruction process of surface layers of friction solids, which leads to a decrease of solid sizes (wearing) in the direction perpendicular to the friction surface [21]. Wear resistance of materials is a characteristic determining ability of these materials to withstand wear under certain conditions of external influence. Types of wear are diverse. They are determined by the variety of changes occurring in the contact layer during friction. Both geometrical contact pattern and properties of contacting surfaces are exposed to these changes [22].

Studying physical patterns during wear of materials is complicated by the fact that during friction surface layers of friction parts are subjected to a strong influence of the external environment with simultaneous mechanical influence of the contacting surface. Physical and mechanical properties of the surface layer may differ depending on properties of material presented in the volume of the part (component) due to surface phenomena (related with adsorption, oxidation *etc.* and conditioned by the intermediate environment), as well as due to stresses in the elastic and plastic area repeatedly occurring in places of actual contact. These stresses and plastic deformation associated with them often lead to a profound change in the surface properties up to change in its chemical composition and phase composition [20].

In practice, one type of destruction of a worn surface can be rarely found, usually several types of wear occur simultaneously but one of these types is the leading one as for the rate of the process.

Wear occurring during friction of material that has come into chemical interaction with the environment is determined as corrosion-mechanical wear. In this case, destruction of the friction surface occurs as a result of two simultaneous processes: corrosion and mechanical wear. Mechanical wear can then take place both during friction of the bonded surfaces and during interaction with the flow of the environment (fluid or gas, which may contain solid parts) [21].

Abrasive wear is one of the most widespread types of material surface destruction in conditions of coal hydraulic mining, coal hydraulic

transportation and beneficiation during operation of equipment used in the field of ore mining industry, cement industry, and energy generating industry. During a long period, hardness of material was the main criterion of its abrasive wear resistance. At the same time, numerous experimental works convincingly proved ambiguity of influence caused by hardness on the abrasive and impact-abrasive wear of metals. An abrasion-resistant material must have certain mechanical and technological properties and in some cases even such properties as erosion and corrosion resistance. Ability of a material to withstand wear is a structurally sensitive characteristic, *i.e.*, it depends on the structure determined by the chemical composition. Structural peculiarities of abrasion-resistant materials include the need to obtain a heterogeneous structure consisting of solid inclusions arranged in a plastic base (matrix). The most important factor determining the resistance of materials to wear is the bonding nature of individual structural components. Solid inclusions are firm only if the type and size of crystal lattices are close enough [23].

Abrasive wear is the main type of wear of machine parts (components) operating in technological environments which contain solids. Wear rates under these conditions are high: 0.1–100 μm/h. Impellers and armoured disks of centrifugal sand pumps operating in the harshest conditions of hydroabrasive wear at mining plants where non-ferrous metals are processed have even greater wear rates [21].

Mineral particles with high hardness usually have non-metallic atomic bonds determining a small volume of adhesion, so soaking in abrasive wear conditions is practically excluded and processes leading to wear in such conditions are in a sense simpler than in conditions of dry friction and boundary friction [24].

Due to the high concentration of contact stresses, the rate of abrasive wear is several orders higher than in other friction conditions, excluding rare cases of soaking. Therefore, abrasive wear is usually leading one in case of combining several types of wear and suppresses them [25].

Causes of surface destruction during abrasive wear commonly include normal and tangential components of the impact impulse of abrasive particles. Dependence of cast iron abrasive and impact-abrasive resistance on microhardness of its metal base is linear. At any content of carbon, the maximal abrasive and impact-abrasive resistance is typical for cast irons with martensitic structure of their metal base [26].

The pattern of destruction under influence of an abrasive material and dependence of wear resistance on the state of the metal are dramatically complicated in transition to heterogeneous alloys with a large difference in properties of their structural components. White wear-resistant cast irons are those very heterogeneous alloys. The metal base of white cast irons may be with certain modifications viewed as alloyed steel of the respective composition, carbides as a fragile phase with par-

tially non-metallic bonds, high hardness, and low plasticity. These structural components of white cast irons differ dramatically in their hardness, plastic deformation ability, and nature of destruction. Therefore, conditions of the destruction mechanism change for the basis and carbides are in various ranges of wear process characteristics [20].

White wear-resistant cast irons (including alloyed ones) may have a much higher wear resistance (in comparison with steel) under favourable combination of abrasive hardness and strength movement rate and angle of attack. *Vice-versa*, under conditions causing intensive fragile destruction, the wear resistance of white cast irons is lower than that of steel. In the process of wearing, transition to intensive destruction of the surface layer of a white wear-resistant cast iron usually takes place abruptly and cannot be explained by any of the factors influencing the process of wearing [11].

Exclusively, the type of abrasive wear determines conditions of fragile destruction of a white wear-resistant cast iron. Inside each of the main types of abrasive wear (in the abrasive mass with abrasive material between the friction surfaces, in the flow, on impact), the threshold of fragile intensive destruction of a white wear-resistant cast iron is either achieved by means of a combination of the respective conditions or not. Depending on this, the range of durable white cast iron is exceptionally wide. As the flow rate, mass of particles and abrasive hardness increases over a certain limit gas-abrasive wear of white wear-resistant cast irons acquires similar to those of wear on impact with an abrasive. Wear in an abrasive mass and hydroabrasive wear at slow movement rates, tangent flow and absence of additional influence caused by the environment provide results analogous to results of tests performed in conditions of friction on sandy abrasive material at low stresses [27].

Analysis of wear resistance relations with the microstructure gives an opportunity to perform qualitative assessment of the role of structural components in the resistance of white cast irons to abrasive wear [20]. Wear resistance of white cast irons depends on the type, amount, dispersion and nature of carbide distribution as well as on structural components of the metal matrix. The greatest resistance to impact-abrasive loads in mills is typical for cast-iron balls with martensite, bainite, residual austenite, and special carbides in their structure. Cast iron wear resistance grows with increase of Me_7C_3-, $Me_{23}C_6$-type (*Me* denotes a metal) carbides in its structure (microhardness of these carbides reaches the level of 2500 HV). Amount of carbides in cast iron grows with increase of carbon content and contents of carbide-forming elements (Cr, Mo, *etc.*) As their total content reaches the 10% -level, alloyed cementite of $(Fe,Cr,V,Mo,W,Ti)_3C$-type is mainly formed; the microhardness of this cementite increases from 800 HV to 1200 HV. With further increase of carbide-forming elements, first hexagonal carbides of Me_7C_3 type are formed (their microhardness is up to 2000 HV), and then carbides of $Me_{23}C_6$ type (with

microhardness of up to 2300 HV) and interstitial phases of Me_nC_m type (with microhardness of up to 3200 HV) are formed. The higher carbide phase dispersity and microhardness, the higher cast iron wear resistance is. At the same time, from the point of impact resistance, the austenite–sorbate–martensite matrix is the most favourable, since martensite itself is known to ensure a high wear resistance of the metal base and viscous austenite–sorbite compound is a high resistant to impact loads preventing chipping of highly wear resistant carbide phase [28].

In addition to properties of own Me_3C and Me_7C_3 carbides, an important role in improving wear resistance belongs to differences in structure morphological properties of cast irons with carbides of these two types. The solid carbide framework of cast irons with ledeburite-type carbides is less wear resistant than the branched austenite-chromium eutectic with dispersed carbide phase of Me_7C_3 type. It is obvious that fragile destruction conditions caused by excess of the load rate in points of actual contact or by the abrasive particle impact energy are created earlier for the solid framework of ledeburite-type carbides than for $\gamma + Me_7C_3$ eutectic [29].

It is difficult to separate the effect of carbide hardness on wear resistance from the influence of their mutual location in chromium cast irons because substitution of a weaker less solid Me_3C carbide with a harder and more solid Me_7C_3 carbide occurs simultaneously with the change of eutectic crystallization mechanism. Therefore, advantages of Me_7C_3 carbides in comparison with Me_3C carbides and, accordingly, advantages of high-chromium cast irons in comparison with low-chromium ones are determined by the both favourable factors, namely, the increase of carbide hardness and the change in the eutectic structure, because these processes occur simultaneously [20].

Composition of carbides plays an important role in the process of abrasive wear of white cast irons. Small amount of proeutectoid constituent (5–7%) weakly increases the abrasive resistance. Increased amount of Me_7C_3 carbides up to the level of ≈30% leads to an increase of relative wear resistance coefficient K_1 according to linear law. This amount of carbides corresponds to cast iron carbon contents of 3.2–3.4%. Further increase of carbon contents and amount of carbides does not lead to increase of wear resistance [30].

Wear resistance of white cast irons significantly depends on the size of structural components, which is determined by the casting cooling rate during crystallization. Size of carbides in wear-resistant white cast irons depends on the degree of cast iron eutecticity. Initial carbides $(Cr,Fe)_7C_3$ in an eutectic cast iron are quite large even in castings of small thickness crystallized at high cooling rate [31].

Maximal amount of $(Cr,Fe)_7C_3$ carbides in cast irons of eutectic composition is of about 30–35%. It is not practicable to obtain a greater amount of carbides and at the same time to preserve morphology of $(Cr,Fe)_7C_3$ carbide

in breakeven conditions of cast iron crystallization. If content of carbon and chromium is increased within the range of this carbide, the structure is carbonized through the growth of large initial carbides presented in form of long hexagonal prisms. Their size is tens of times the size of eutectic carbides. Such large fragile carbides in the structure cause decrease of wear resistance. If the content of carbon is increased, the remaining within the range of eutectic composition amount of carbides will increase but at the expense of $(Cr,Fe)_3C$ carbides. At the same time, resistance to abrasive wear does not increase due to low hardness of cementite in comparison with chromium carbides as well as due to a less favourable structure of ledeburite-type eutectics [32].

The presence of carbides in the structure of white cast irons is a necessary but not a sufficient condition determining their high wear resistance. The metal base does not itself resist the destructive action of an abrasive but serves as a bond and support for highly solid carbides in the natural composite material [33].

The metal base must satisfy several requirements: soaking carbides as tightly as possible under conditions of abrasive grain load; ensuring minimal deformations in order to prevent carbides from cracking and chipping; detentions of the base sections between carbides should be small enough to minimize selective wear of the base caused by the abrasive material, as well as denuding of carbides, their washing out and edge-chipping [20].

Ferrite and ferrite–carbide mixtures are the least suitable to meet these requirements; the same is true about stable austenite, which is not prone to martensite transformation in the process of wear. Martensite and residual austenite unstable under these conditions of wear are the most suitable to meet the requirements set to the metal base [12].

Operation under conditions of impact-abrasive wear may lead to an intensive fragile destruction of white wear-resistant cast irons. Such destruction occurs when limit values determined for the rate of microvolume loading with the energy of abrasive particle impact are exceeded. An important role under such conditions is played by size of carbides and their orientation in respect to the surface worn. It is obvious that under conditions of load up to limit values, the wear rate depends on the processes of plastic deformation of the base; carbides are removed in the process of their gradual wear if deformations of the base are small or with the base after previous destruction if deformations are large. Surface destruction starts from the metal base. After the boundary load conditions are exceeded, the surface destruction starts from carbides: they are chipped intensively with further destruction of the metal base [34].

In conditions of abrasive wear complicated with surface softening of the white wear-resistant cast iron stipulated by electrochemical processes in the electrolyte environment and by surface effects, an important role is at-

tributed to thickness of the film of environment influence products as well as by depth of abrasive penetration. If depth of penetration is significantly greater than the layer with changed properties, the requirements to the structure determined for conditions of ordinary abrasive wear remain valid. If not, the corrosion resistance of the material, strength and hardness of the corrosion products are crucial [35].

Using white wear-resistant cast irons instead of steel 110G13L for production of high wear parts of crushing and grinding equipment gives an opportunity to increase their service life [36].

Selection of rational cast iron alloying is possible based on correct ideas about quantitative ratio of proeutectoid constituents, their morphology, and nature of metal base alloying, *i.e.* alloy matrix providing maximal wear resistance under conditions of abrasive wear. The maximal relative wear resistance of cast irons is ensured by means of obtaining an austenite–martensitic structure in the matrix containing metastable austenite in the concentration of approximately 0.6% C, transformation of this austenite into deformation martensite in the process of wear contributes to creation of a wear-resistant dissipative structure with the greatest microhardness of the operating surface [37].

2.5. Compositional and Structural Effects on the Wear Resistance of High-Chromium Cast Irons

The main service property of white cast iron consists in its wear resistance. Other properties (including mechanical, foundry, technological properties *etc.*) are auxiliary properties and determine the limits of applicability and the possibility of using different grades of white wear-resistant cast iron.

Wear resistance of numerous materials is assessed based on researching their properties at various test conditions. Diversity of research methods, materials used as standard ones, and other factors leads to the fact that the data on wear resistance of various cast irons become incomparable, and the choice of the optimal alloy grade for specific operating conditions is difficult [38].

As a result of friction, many parts of machines are subjected to the wear. Processes leading to the wear are called wearing (wear and tear). In the result of wear dimensions of worn parts change, the gaps between the friction surfaces are increased and that causes beats and knocks.

The mechanisms of wear along with regularities of friction conditions and material properties of parts were analysed by the international group of scientists in Refs. [25, 34, 36, 39–41]. Their results gave an opportunity to reveal the main factors determining intensity of wear and durability of parts and machines, and in some cases create calculation methods.

Abrasive hardness is one of the main factors. Quartz sand with microhardness of 800–1100 HV is the most common abrasive, which has a destructive effect on the operating surfaces of machine parts used in the field of mining industry, industry of building materials, and agricultural industry.

Microhardness of about 600 HV should be considered as the critical value of metal hardness in case of wear by means of quartz sand. In this range of hardness, the change of wear mechanism occurs: direct destruction by means of cutting or tearing is substituted with repeated deformation or destruction in the result of polydeformation process; wear resistance increases dramatically.

In addition to abrasive hardness, factors that have a great influence on the intensity of wear include size and shape of particles and degree of their fixation. As the size of particles and sharpness of their angles increase (as lug radii decrease) and as level of fastening increase, the wear intensity increases as well [42]. In addition to that, the conditions of wear and tear with the flow of abrasive particles in a liquid or gas are described by means of concentration of the abrasive in the flow, rate of impact caused by particles and the angle of inclination of this velocity vector to the surface of the component (angle of attack, α). Dependence of the wear intensity on the flow rate is static: $Ig = kV^m$. Here, Ig is the mass loss per 1 kg of the abrasive that has contact with the component surface; k is the coefficient depending on the properties of the abrasive, the material of the component, and the angle of attack; V is the flow rate (velocity). Sensitivity of the material worn to the abrasive velocity may vary significantly, but in all cases $m > 1$, *i.e.*, wear increases faster than the flow rate. The degree of m for velocities up to 100 m/s increases with the brittleness of the material and is 2.3 for St3 steel, 2.5 for hardened steel 45, 2.8 for white cast iron, and 2.9 for basalt [25, 42].

The pattern of destruction under influence of an abrasive material and dependence of wear resistance on the state of the metal are dramatically complicated in transition to heterogeneous alloys with a large difference in properties of their structural components. White wear-resistant cast irons are those very heterogeneous alloys.

The authors of Ref. [43] researched relationship between the characteristics of the carbide phase of high-chromium cast iron and its hardness, coercive force, because the wear resistance of high-chromium cast iron depends on many factors and, first of all, on the characteristics of the carbide phase. Authors [43] examined the samples selected from the top rings of the centrifugal roll barrels.

Amount of the carbide phase K_{ph} is one of the main parameters determining properties of high-chromium cast iron. In cast irons with $(Cr,Fe)_7C_3$ carbides, the amount of carbides K_{ph} can be calculated accord-

ing to the following formula:

$$K_{ph} = 12.33C + 0.55Cr - 15.2. \quad (1)$$

The experimental data are in good agreement with the calculated values of K_{ph} for castings obtained by centrifugal casting of these cast irons. After statistical processing of the obtained data, we have found out that for the studied samples, the K_{ph} value is in the range of 23.1–33.5% and averages 28.2%. According to the results of researches, the dependences of HS hardness were obtained, this hardness was determined according to Shore method. It was determined that as the K_{ph} grows, the hardness and coercive force increase.

In conditions of abrasive wear, the high wear resistance can be ensured, if the white iron carbide phase complies with the following terms:

• the maximum amount of carbides is retained with hardness exceeding the abrasive hardness;

• branched carbide phase is evenly distributed in the metal matrix; preferably the maximum amount of eutectic is provided;

• Me_7C_3 carbides are axially oriented to the perpendicular surface, they are being worn;

• the carbides have a minimum size, usually unacceptable eutectic carbides.

The metal base must satisfy the following requirements:

• soaking carbides as tightly as possible under conditions of abrasive grain load;

• ensuring minimal deformations in order to prevent carbides from cracking and chipping;

• retentions of the base sections between carbides should be small enough to minimize selective wear of the base caused by the abrasive material, as well as denuding of carbides, their washing out and edge chipping.

Ferrite and ferrite–carbide mixture are the least suitable to meet these requirements; the same is true about stable austenite, which is not prone to martensite transformation in the process of wear. Martensite, bainite, and residual austenite unstable under these conditions of wear are the most suitable to meet the requirements set to the metal base [41].

In Ref. [44], the author demonstrated that wear resistance of a white cast iron depends on the type and amount of carbides, their dispersity and branching as well as on the metal matrix components. The greatest resistance to impact of abrasive loads occurring in mills can be provided by the microstructure of cast iron balls containing martensite, bainite, troostite, sorbite, austenite, and special carbides. Cast iron wear resistance grows with increase of Me_3C_7- and Me_3C_6-type

carbides in its structure (microhardness of these carbides belongs to the range 800–2500 HV).

Amount of carbides in a cast iron grows with increase of C content and carbide-forming elements Cr, Mo, V, Ti, and W. As their total content reaches the level of 8%, the alloyed Me_3C cementite is mainly formed; the microhardness of this cementite increases from 800 HV for Fe_3C to 1200 HV for alloyed cementite. With further increase of the content of carbide-forming elements, first, the Me_7C_3 hexagonal carbides (with microhardness of up to 2000 HV) are formed. Then the $Me_{23}C_6$ carbides are formed with microhardness of up to 2500 HV and interstitial phase of Me_nC_m type with the microhardness of up to 3200 HV, *e.g.*, VC (3000 HV), WC (2200 HV), Ti (3200 HV), Mo_2C (1500 HV). For comparison, martensite has a microhardness of up to 1000 HV, the microhardness of a high-alloyed austenite is 300–600 HV, and that of low-alloyed austenite and pearlite is 250–320 HV. The more solid, more dispersed and more insulating the carbide phase, the higher the durability and viscosity of the cast iron is.

The metal base of white cast irons may be viewed as alloyed steel of the respective composition, carbides as a fragile phase with partially non-metallic bonds, high hardness, and low plasticity. These structural components of white cast irons differ dramatically in their hardness, plastic deformation ability, and nature of destruction. Therefore, conditions of the destruction mechanism change for the base and carbides are in various ranges of wear process characteristics. So, values of abrasive critical hardness (taking into account the ratio H_m/H_a (where H_m is a hardness of the tested material, H_a is an abrasive hardness), at which the linear relationship of wear and material hardness are disturbed) are different for the base and the carbides. The article [41] represents data on the critical hardness of an abrasive capable of intensive cutting high-chromium cast iron martensite, 1100–1450 HV. For carbides, it is significantly higher: for cementite it is 1600 HV, and for $(Cr,Fe)_7C_3$ carbide it is above 2000 HV. For soft structural components of the metallic base (ferrite, products of diffusional decomposition of austenite with microhardness up to 300–400 HV), critical values of abrasive hardness are reduced to 500–650 HV, *i.e.*, below hardness of quartz being the most common abrasive.

In the case of studying solid abrasive (Si), the difference in the microstructure of the base and the type of white cast iron carbides appeared to be insignificant, since all structural constituents are obviously destroyed by means of cutting or tearing off, since H_a is much higher than the microhardness of all structural constituents. In case of usage of an abrasive of a lesser hardness (garnet), the difference in microhardness of structural components plays an important role. It is evident that under these research conditions, the garnet is not able to scratch carbides

of the Me_7C_3 type; silicon carbide is equally easily introduced and scratches both carbides and metal components of white cast irons.

White wear-resistant cast irons (including alloyed ones) may have a much higher wear resistance (in comparison with steel) under favourable combination of abrasive hardness and strength movement rate and angle of attack. *Vice-versa*, under conditions causing intensive fragile destruction, the wear resistance of white cast irons is lower than that of steel. For instance, at a velocity of 100 m/s, an angle of attack of 30° and wear by means of glass particles (≈500 HV), the wear resistance of chromium–molybdenum cast iron is more than 40 times higher than that of steel 45. At $\alpha = 90°$, it is about 15 times higher. In the flow of quartz particles (1100 HV) and at an angle of $\alpha = 90°$, the wear resistance of this cast iron is 1.6 times lower than that of steel 45. At an angle $\alpha = 30°$, the wear resistances of these materials are equal.

2.6. Effects of Alloying Elements and Heat Treatment on the Operational Properties of Sparingly Doped High-Chromium Alloys

The structure of alloyed cast iron with special properties, their operational and mechanical characteristics are determined by the chemical composition and first of all by the content of alloying elements.

The level of alloying determines different special properties of cast iron castings: wear resistance and corrosion resistance, paramagnetism, cold resistance, low or high thermal expansion coefficient. Special and mechanical properties of cast iron (according to the state standard GOST 7769-82) are checked periodically if needed for technical conditions since these characteristics are optional [45].

Effect of alloying elements on the properties of white cast irons is quite significant. Alloying elements largely determine the type of carbide and the metal base of white cast irons. Chromium is one of the main alloying elements for white cast irons.

Chromium is an element that promotes strong bleaching of cast iron. It decreases solubility of carbon in α-iron and γ-iron, increases the degree of the solid solution stability and the amount of the eutectic component. Even with a small content of chromium, a chromium-saturated carbide phase of the cementite type is formed in cast irons [46].

Properties of Fe–Cr–C are determined by two important peculiarities of chromium as an alloying element, namely, limitation of the γ-range and formation of carbides.

The high affinity of chromium to carbon causes the formation of not only cementitious type carbides, but also more resistant special chromium carbides in the structure of chromium steels. At relatively low content of chromium in steels, iron carbide, *i.e.* cementite (Fe_3C), is

formed, and up to 18–20% of Cr, it can be dissolved in it. Chromium alloys form special chromium carbides $(Cr,Fe)_7C_3$ and $(Cr,Fe)_4C$. Trigonal chromium carbide $(Cr,Fe)_7C_3$ dissolves from 30 to 50% of Fe, and cubic carbide $(Cr,Fe)_4C$ dissolves up to 35% of Fe.

The more carbon in the alloy, the greater concentration of chromium are needed for formation of $(Cr,Fe)_7C_3$ and $(Cr,Fe)_4C$ carbides. So, to eliminate the formation of cementitious-type $(Fe,Cr)_3C$ carbide, at carbon content of less than 1%, 5–6% of chromium are sufficient; and at 2% of C, less than 17–18% of Cr are needed. Due to the decrease of carbon solubility in austenite under the influence of chromium alloying, the line of maximum solubility of carbides in austenite and at the same time the eutectoid point are shifted to the left towards smaller concentrations of carbon. The γ-range in steels narrows under the influence of chromium, but since after forming carbides carbon removes chromium from a solid solution, the more chromium is required for the complete exclusion of austenite in the structure of the Fe–Cr–C alloy, the more carbon in the alloy. Thus, the complete disappearance of the γ-range in steel with 1% of carbon occurs when the chromium content exceeds 30%, whereas in carbon-free Fe–Cr alloys 12% of Cr is sufficient to obtain a purely ferrite structure. As chromium content increases, the eutectic point shifts to the left.

In cast iron with 8.85% of Cr, alongside with cementite, a significant amount (about 18%) of more solid carbides $(Cr,Fe)_7C_3$ is retained that leads to an increase in wear resistance. Increase of chromium content up to 10–12% leads to formation of carbides (mainly those of trigonal type with a microhardness of 1240–1550 kgf/mmI. This causes a sharp increase of wear resistance. The maximal wear resistance is typical for cast irons with 12–24% of Cr, which include carbides of Me_7C_3-type. Increase of Cr content up to 29% at 3% of C results to a decrease in wear resistance because large brittle needles of eutectic carbides appear in the cast iron.

With the increase of microhardness of carbides from 1000–1100 to 1240–1700 kgf/mm^2, the wear resistance of cast iron worn by means of a quartz-type abrasive increases significantly. The harder the carbides, there is the higher wear resistance of chromium cast irons [47].

As known, the bleaching enhancers can be arranged in the order of increasing effectiveness of their effect as follows: Mn, Mo, Sn, Cr, V, S, and Te. Therefore, below, we consider the effect of separate alloying elements on properties of white wear-resistant cast irons.

Silicon in a white cast iron can be viewed as an alloying element, which is distributed during crystallization between austenite and eutectic melt. Silicon raises the temperature of eutectic crystallization, widens the eutectic transformation interval, preventing overcooling, and it also reduces the effect of cooling rate.

With a content of 0.5 to 1.5%, silicon increases the upper critical bleaching rate of cast iron, *i.e.*, it reduces cast iron bleaching.

Silicon has a very strong influence on the process of forming the casting structure, both during solidification and during structural changes in the solid state. According to analyses of silicon distribution between the phases in white cast irons, it was determined that at high cooling rates of the workpieces, it is almost completely concentrated in the matrix (ferrite).

Manganese facilitates stabilization austenite and cementite in white cast irons. Studies of the distribution of Mn, Cr, Mo, and V in white cast iron at an amount of each element of about 1.0% and a carbon content of 1.8–3.8% showed that the concentration of the alloying element in the dendrites is minimal in the middle, gradually increases towards the periphery, and it is much higher in eutectic cells. As manganese content increases, the redistribution of carbon between austenite and eutectic melt can be observed in the direction of increasing carbon content in austenite.

Nickel and carbon form metastable Ni_3C carbide. Eutectic is formed in the C–Ni system. The maximum solubility of carbon in nickel in the solid state is about 0.55%. Nickel alloying of cast iron facilitates austenite stabilization and widens γ-Fe range. In the result of investigations, it was determined that the Ni influence on hardness and wear resistance of white cast irons is similar to that of Mn. The strongest nickel influence is caused when concentration of this element is up to 3%.

At small concentrations of nickel (up to 1.3%), dendritic structure of cast iron is observed alongside with very large fields of a troostite-forming eutectoid with inclusions of secondary cementite and eutectic of a thin structure.

With the increase of Ni content up to 3.43%, one can observe the appearance of austenitic structure with large-needle martensite.

Thus, the influence caused by nickel is to a certain extent analogous to that of manganese: increased nickel content leads to inhibition of diffusion decomposition of austenite, appearance of austenite–martensitic structure, tendency to formation of continuous cementitious ranges is observed. However, nickel influence is more effective.

Molybdenum and carbon form several carbides. According to data of different studies, carbon solubility in molybdenum in the solid state is 0.1–0.3%. Molybdenum and iron form solid solutions and several chemical compounds. Researches of white cast irons with Mo contents of 0.09–1.21% Mo demonstrated that molybdenum is completely concentrated in the carbide phase; it was not found in the ferrite.

As determined in Ref. [19], the molybdenum influence on white cast irons is especially significant at contents of 0.5%. The main role of molybdenum in white cast irons consists in an enhancement of their hard-

enability. As molybdenum content grows up to 0.49%, the eutectoid becomes thin-plated and troostite appears.

As regards the copper influence, minimal solubility of Fe in Cu is 3.4%, and solubility of Cu in Fe at a temperature of 1100 °C is 10%. As a temperature decreases, the concentration of copper in the solid solution also decreases and equals to 0.35% at a temperature of 700 °C. In the result of adding copper to a white cast iron, the resistance to the loading improves. At Cu content of 0.6%, a dendritic structure was observed alongside with a thin-plate and troostite-forming eutectoid with inclusions of secondary cementite, a considerable amount of thin-structure eutectic and large sections of structurally free cementite.

By means of copper alloying, the hardness and wear resistance of white cast irons can be improved. A great effect can be expected if copper is introduced in combination with other alloying elements (nickel, chromium, vanadium) [47].

Correct selection of heat-treatment regime for white high-chromium cast iron will give an opportunity to achieve an improved complex of mechanical and operational properties of products operating in conditions of impact-abrasive wear.

The author of Ref. [29] demonstrates that an efficient improvement of operational properties of alloyed cast iron balls can be achieved through applying the heat treatment (HT). Influence on the structure and properties of balls of various diameters produced by means of poring cast irons of various compositions to the casting mould and applying various kinds of heat treatment:

• normalization from a heating temperature of 950 °C, 1000 °C, and 1050 °C after soaking for 4 h;

• with further drawing-back with heating up to 300–400 °C and soaking time of 4 h, and with heating up to 600–700 °C and soaking time of 6 h.

Analysis of the microstructure and properties of thermally treated cast iron balls shows the following:

• the microstructure of casted balls is presented as a very large and strongly branched eutectic carbides in the metal matrix, the matrix consists of austenite (*A*), sorbate (*S*), troostite (*T*), martensite (*M*), bainite (*B*) in different proportions depending on the chemical cast iron composition and size of balls;

• heat treatment of balls produced of all alloyed cast irons results in a significant improvement of all properties due to the crushing and coagulation of eutectic carbides, the formation of secondary carbides and the dispersion of the matrix structural components;

• heat treatment of balls with high content of Mn results in a decrease in their hardness and wear resistance due to increased amount of austenite in their microstructure, the balls become nonmagnetic;

• the best properties of the balls are achieved for Cr–Ni–Mo: a cast iron with normalization from 1050 °C, drawing back at 700 °C for 6 h, which ensures crushing of eutectic carbides and secondary carbides newly formed in the matrix, dispersing the components of the matrix;

• normalization of the balls without further drawing back does not actually affect the improvement of ball operational properties.

The authors of Ref. [48] investigated an influence of casting thickness and heat treatment regimens on the structure and properties of cast iron MCH15 alloyed with the usage of 15% of Cr and V. If the heat treatment is selected properly, the residual tensile stresses in the transition zone are minimized shifted to the internal, less stressed sections. All castings were subjected to a preliminary diffusion annealing according to the following regime: heating in a furnace from 50–100 to 1050 °C with a soaking time of 6 h, slow cooling in the furnace (with closed doors) down to 100–200 °C. The workpieces were then heated up to 950 and 1050 °C with further cooling in water, oil, in the air, in water, and then in oil, in water down to 400–300 °C, followed by transfer to the furnace heated up to 250–300 °C, for isothermal soaking during τ = 2 h. The maximum hardenability depth for castings made of cast iron MCH15 (according to the thermokinetic diagram) is 125–65 mm when cooled in water, 110–35 mm when cooled in oils, and 25–5 mm at cooling in the air.

According to the research results, it was determined that different regimes of heat treatment practically do not change the composition and physicomechanical properties of the carbide phase of a white cast iron of given chemical composition. However, different regimes of heat treatment can change the hardness of the matrix, slightly affect the volume fraction of the carbide phase and greatly change the shape of the phase components. Increased microhardness of the base increases the microhardness of the cast iron. Changing the morphological form of the phase components significantly changes the tendency of castings to formation of cracks, both during heat treatment and during operation in the composition of finished products, due to presence or absence of structural stress concentrators. Evaluation of wear resistance of cast iron in different structural states demonstrates that when the microhardness is changed from 55 to 60 HRC, the cast iron wear resistance does not change; but with a decrease in hardness down to 53 HRC, the wear resistance decreases by ≈5–10%; and at a hardness of 40 HRC, it decreases by 30%.

The article [49] reports on data concerning the maximum and minimal wear resistance of high-chromium white cast iron. The maximum of the wear resistance was obtained after heating at a temperature of 1100 °C, cooling down to 350 °C with soaking at this temperature and further cooling in the air, and after stabilization heat treatment at 780 °C with cooling in the air. The minimal wear resistance and corro-

sion resistance were obtained after hardening in oil and drawing back at 500 °C. In terms of the microstructure, the highest wear resistance is typical for the cast iron with uniformly distributed carbides in a softer matrix.

The amount of residual austenite in the white cast iron with 12% of Cr strongly depends on the carbon and manganese content: C reduces an amount of residual austenite, while Mn increases this amount. In the process of 450–550 °C drawing back of samples hardened from 1100 °C, the hardness grows due to release of Me_7C_3 dispersed carbides in the austenite matrix and further partial transformation into pearlite and martensite at cooling down to the room temperature.

High strength, viscosity, and hardness of (58 HRC units) are obtained in the high-alloyed white cast irons after austenization at 900 °C, 50 minutes, and drawing back at 200 °C, 4 h. During this process, their structure is flattened, carbides are distributed more uniformly, and thermal stresses are dramatically reduced.

According to the U.S.A. standards, the typical composition of white cast iron is as follows: 2.4–3% C, <1% Si, 0.5–1.5% Mn, 11–28% Cr, 0.5–1.5% Ni, 1.2% Cu, 0.5–1.5% Mo. Composition of carbides is Me_6C, $(Fe,Cr)_7C_3$, and if V is available, VC is also presented. In the as-cast state, the matrix has an austenitic structure. Annealing at 850–950 °C with cooling in the furnace down to 720–700 °C, with soaking for τ = = 5–20 h and cooling in the air ensures formation of a pearlite matrix with the hardness of 300 HV. After unbalancing at 1000 °C, the structure is presented by carbides located in a martensitic matrix. Fracture toughness K_{1c} reaches 20–25 MN/m$^{3/2}$ at a martensitic matrix; and if residual austenite is available, fracture toughness reaches the level of 25–30 MN/m$^{3/2}$.

A significant increase in impact toughness of the white cast iron with 12–28% of Cr (≤18 J/cm^2) can be achieved by means of hardening from >1150 °C, during which carbides are partially dissolved in austenite and their boundaries are rounded; however, it is a technologically difficult procedure.

2.7. Contemporary Trends in Development and Application of the Wear-Resistant Cr–Mn–Ni Alloys

State-of-the-art constructional materials often operate under difficult conditions of mutual influence of friction forces, corrosion, abrasive, and impact-abrasive wear; so, they have to possess certain physical, mechanical, and physicochemical properties, and meet a number of requirements, which are often contradictory.

High level and complex of properties at low cost can be provided using the sparingly alloyed manganese alloys [50]. When changing the

heterogeneity of the structure, depending on the functional purpose of the alloy by means of rational alloying and applying different regimes of heat treatment, the formation of the required properties of manganese cast iron can be affected intentionally.

The most common manganese alloy widely used for the casting of castings (lining plates of ball mills), is Hadfield steel 110G13L [48]. Currently, castings of this steel are performed in accordance with the state standard GOST 977-88 with the specified mechanical properties (Table 1). Having a high complex of mechanical properties, this steel may not always satisfy consumers' requirements, especially concerning abrasive resistance [52].

In addition to 110G13L, the state standard GOST 977-88 defines the following grades of Mn steels: 110G13H2BRL, 110G13FTL, 130G14HMFAL, and 120G10FL. These steels contain a large amount of alloying elements, so it is urgent to replace them with sparingly doped alloys with a high level of abrasive resistance and impact-abrasive resistance.

Authors of Ref. [53] proved the fact of extremely high resistance of metastable austenitic alloys during cavitation wear. They also identified a new field of metastable austenite application for increasing surface resistance of materials to contact dynamic load occurring during mechanical types of wear.

Subsequently steels with an extremely high complex of mechanical properties were created; these properties are provided with metastable austenite and presuppose availability of manganese as an alloying element. However, these steels being alloyed with a large amount of chromium, molybdenum and nickel cannot be used in mass production. The principle of austenite metastability during creation of wear-resistant manganese alloys was then substantiated in Refs. [54, 55].

The idea of using a metastable structure to increase the service properties of materials has been further developed in works of many researchers. In the monography [56], authors proved an increase of the wear resistance at abrasive wear of steels with structure of metastable austenite (from the perspective of the energy theory). Reaction of a metal to the influence of the abrasive solid depends on its structural state and may include processes of strengthening, phase transformation, destruction of interatomic bonds as well as other phenomena. All these processes consume energy transmitted to the metal by the abrasive solid. The destruction occurs when the metal absorbs energy of the limiting value, which is determined by the bonding forces in the metal and the energy intensity of structural transformations.

The process of martensitic transformations during wear does not require very high-energy consumption, but plays an important role in improving wear resistance of alloys. Formation of deformation martensite leads to occurrence of internal compression stresses in the volume

of metal subjected to martensitic transformations. Energy of abrasive interaction is consumed for overcoming these stresses and respectively consumption of energy for metal destruction decreases.

The principle of composite hardening of wear-resistant alloys was formulated and applied in Ref. [57]. Role of structural factors in the formation of structure and properties of these alloys was demonstrated; this role is especially evident in the grain compositions. In addition to direct interaction of dislocations with reinforcing particles, grain boundaries and subgrain boundaries are of great importance in compositions of this kind (they make an additional contribution to increasing strength).

In References [58, 59], the principles of creating economically metastable multifunctional alloys and reinforcing technologies were substantiated. They are as follow:

- creation and purposeful use of phase-structural metastability during testing, operation, and treatment of steels and alloys;
- controlled kinetics of deformation and phase transformations during testing and using alloys;
- integrated use of mechanisms of strengthening and formation of special properties;
- complex alloying and interchangeability of alloying elements in designing new metastable steels and cast irons.

Based on the above-mentioned principles, the new sparingly alloyed manganese and chromium–manganese alloys with high wear resistance were created [58, 59].

Currently, extensive works are being performed worldwide aimed at developing and using new manganese steels and manganese cast irons. A high level of abrasive wear resistance (K_a) and impact-abrasive wear resistance (K_i) of manganese alloys has been achieved: see Table 2, where the 110G13L steel level was taken as a unit.

Table 1. **Mechanical properties of castings with section of 30 mm made of 110G13L steel [51]**

$\sigma_{0.2}$, MPa	σ_B, MPa	δ_5, %	ψ, %	Impact toughness *KCU*, J/cm^2	HB, units
360–380	654–830	34–53	34–53	260–350	186–229

Table 2. **Achieved level of wear resistance different alloys [58, 59]**

No.	Alloy grade	K_a, relative units	K_i, relative units	No.	Alloy grade	K_a, relative units	K_i, relative units
1	120G2C2T	1.35	1.04	4	220H2G4	2.8	0.6
2	120G10FTL	1.48	1.4	5	H12F1	4.7	1.47
3	130G7TL	2.1	—				

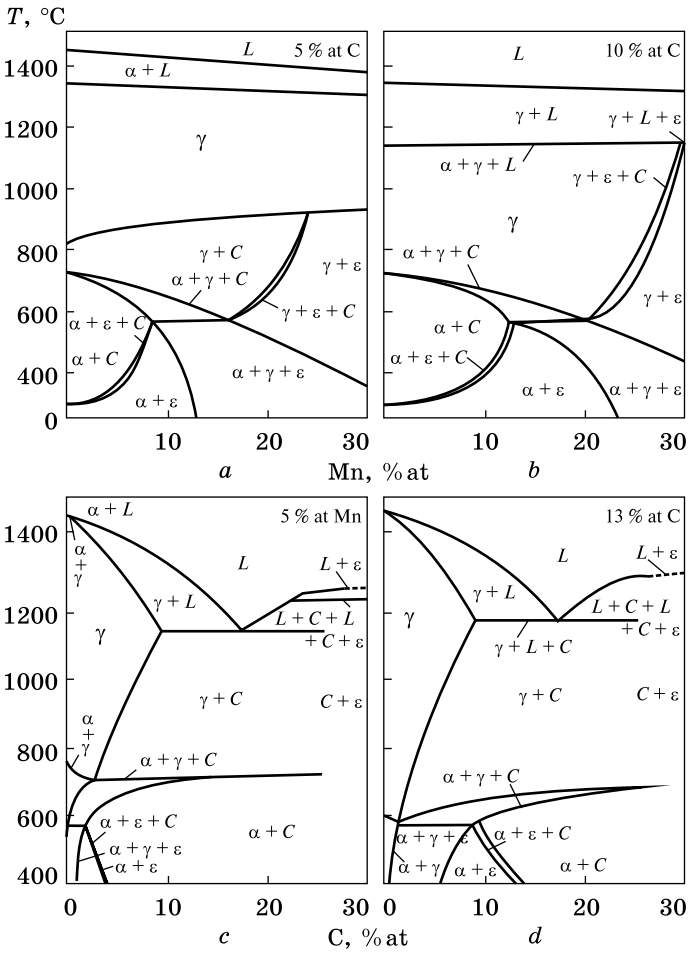

Fig. 1. Sections of the state diagram for the Fe–C–Mn system with eutectoid–peritectoid transformation (*C* denotes cementite) [61]

Manganese steels Nos. 1–3 do not provide a significant increase in the level of wear resistance as compared to steel 110G13L. The greatest level of abrasive wear resistance and impact-abrasive wear resistance is typical for H12F1 steel. However, this steel (analogously to alloys CHH16G4F and CHH17NMFT) contains a significant amount of critical elements (chromium and vanadium), which complicates the widespread use of high-chromium alloys.

As known, carbide transformations may occur in doped alloys of Fe–C–Cr and Fe–C–Mn systems [60]. This is because the cast structure of these alloys is usually nonuniform. With a high-temperature annealing, the iron structure tends to be balanced so unbalanced carbides presented in excess are partially dissolved in austenite and partially converted to carbides of another type.

First of all, this refers to alloyed cementite, which is converted into Me_7C_3 carbide by means of its enrichment with carbon, chromium and

manganese according to the following reaction:

$$3(Fe,Cr,Mn)_3C \rightarrow (Fe,Cr,Mn)_7C_3 + 2\gamma\text{-}Fe(C,Cr,Mn). \quad (2)$$

In the result of this transformation, the amount of alloyed cementite and ledeburite decreases, carbide particles are separated from each other, areas of alloyed austenite are formed, the structure acquires compositional morphology.

The relatively low-temperature eutectoid–peritectoid transformation is of great interest; it can occur in sparingly doped alloys of Fe–C–Si, Fe–C–Cr and Fe–C–Mn systems [61] from the reaction:

$$\gamma\text{-}Fe + K_1 \rightarrow \alpha\text{-}Fe + K_2, \quad (3)$$

where K_1 and K_2 are carbides of different types. The eutectoid–peritectoid transformation in Fe–C–Mn alloys according to Ref. [61] is shown in Fig. 1.

However, until now, the possibilities of eutectoid–peritectoid transformation have not been sufficiently taken into account in forming structure and increasing wear resistance of such alloys. Literature courses provide practically no data on kinetics of the eutectoid–peritectoid transformation, and this complicates justification of the choice of optimal concentration parameters and thermoforming parameters for alloys with high service properties.

2.8. Sparingly Alloyed High-Chromium and Cr–Mn–Ni Alloys for Production of Rolling Tools

Rollers are the main tool for rolling mills. Material and method of manufacture of rollers largely determine the quality of rolled metal, including its surface quality and accuracy of its profile and size, frequency of roll change on the mill, the number of roll remachinings, their specific costs and the complexity of processing. The influence of tool material heat resistance and oxide scale formation processes on the surface of rolls and the quality of the obtained products is indisputable. The higher the heat-resistance of the tools, the greater their service life, since less tendency to oxide scale formation has a positive effect on wear resistance characteristics. The need to comply with the temperature regimes of rolling leads to the fact that the rolled metal has to be heated to the required temperature. As tools are heated, they have to be cooled intensively. However, despite all precautions, the temperature of the tool at the point of contact with the rolling tool may reach 600 °C and above. Therefore, the main operational properties of rolling tools in addition to wear resistance should include heat resistance and high temperature strength under variable temperature actions.

The main rolling tool has the stability and efficiency, which are determined by the technical and economic performance standards of roll-

ing tools as well as by duration of their continuous operation. The most tools were casted from ordinary and alloyed white cast irons, particularly in composite execution (2- and 3-layered), or with a hardened or bleached surface.

Wear resistance of white cast irons is affected by a great number of factors: chemical composition, crystallization conditions, microstructure, nature of alloyed carbides, *etc*. High wear resistance in conditions of slipping friction is typical for high-chromium (>10–15% of Cr) austenite–carbide eutectic cast irons with ≈30% of carbides. The abrasion resistance of chromium–vanadium cast iron is greater than that of chromium–molybdenum cast iron.

When tested for wear resistance in combination with SiC abrasive, the optimum combination of wear resistance and dynamic plasticity K_{1d} is achieved in low-alloyed vanadium cast iron, low-carbide chromium–molybdenum cast irons with low content of carbides and in chromium–vanadium cast irons. In case of friction in combination with softer materials, a good combination of wear resistance and K_{1d} is observed in V cast irons with release of globular vanadium carbide and in chromium molybdenum cast irons with a small amount of carbides. Electrochemical studies determined that corrosion and wear mutually reinforcing (synergic action) if these materials are exposed to a sludge stream containing solid particles.

The improvement of casting quality needs [62–65] inspection at all stages of production alongside with non-destructive microstructure monitoring, defect pattern diagnostics [66–68], and control. At the same time, the annealing of the products should be ensured and formation of pearlite should be excluded.

Dangerous factors influencing quality of instruments made of hypoeutectic cast irons include carbon enrichment of the upper part of large (5–12 tons) castings and the resulting formation of a crude ledeburite structure and cementite network leading to high-temperature brittleness and formation of transverse cracks.

High-alloyed chromium–molybdenum white cast irons are becoming widely used increasingly due to their high wear resistance and impact toughness. They usually contain 1.3–3.6% of C, ≤28% of Cr, ≤3% of Mo, 0.4–2% of Mn. Their structure consists of chromium carbides, evenly distributed in the martensitic matrix, (hardness >700 HV). In the presence of metastable eutectics based on Me_7C_2 carbide, white cast irons have abnormally high plasticity and resistance to impact-fatigue destruction.

With increase of the microhardness of cast iron metal base with 12–14% of Cr, there is a linear increase of abrasive and impact-abrasive wear resistance. At the same time, with any carbon content, the maximal wear resistance is typical for white cast iron with a martensitic matrix.

Wear resistance of white cast irons with 14–20% of Cr, 1–6% of Ni, and 1–3% of Mo under high stresses is determined by the microhardness of the matrix and carbides, as well as by the shape and distribution of these carbides. Impact toughness of cast irons depends on the distance between carbides as well as on their shape and size. A linear relationship was established between the weight loss during impact-abrasive wear and the amount of carbide phase in white cast irons.

White cast iron with 1.5–3% of C, 12–18% of Cr, and ≤3% of Mn along with Mo hardened from 1050 °C in the air and drawn back at 490 °C (4 h) is in a state, which corresponds to the heat treatment regime of rolling tools (∅ = 700 mm). The maximal compression strength (2800 MPa) is typical for the cast iron with 18% of Cr. Carbon gently increases the strength during flow of white cast irons, chromium causes the opposite action, molybdenum increases plasticity of white cast irons, if compressed carbon lowers plasticity.

White cast iron with optimal operational and technological properties should have high indexes of tribological properties after hardening and processing by means of cutting after annealing. The best mechanical properties are typical for cast iron ICH280H20G3, recommended for production of such high-loaded parts as rotoblast barrel blades.

Concerning wear-resistant white cast irons for rolling tools, there is a large number of inventions intended for further improving their wear resistance, mechanical properties, as well as technological properties and technology of production (including multilayered ones).

Proposed cast irons typically contain 2.5–3.5% of C, ≤35% of Cr, ≤5% of Ni, and ≤3% of Mo. The best properties are achieved after heat treatment of white cast iron products.

Researches performed in the sphere of tool materials are mainly aimed at achievement of high and uniform hardness of barrel surface, strength and contact-fatigue endurance, sufficient depth of the working (active) layer, high wear resistance and favourable distribution of residual stresses.

Thus, wear-resistant white cast irons are very promising and technological material for the manufacture of rolling tools, which become closer in their properties to more expensive steel tools.

2.9. Objectives of the Study

The purpose of this work consists in the following:

(i) developing the new sparingly alloyed wear-resistant materials based on chromium–manganese–nickel alloys;

(ii) researching patterns determining structure formation, phase composition and distribution of alloying elements between phases and structural components of Cr–Mn–Ni alloys in the as-cast state;

(iii) researching regularities of bainitic nanostructured matrix formation in experimental chromium–manganese–nickel alloys;

(iv) determining regularities of influence caused by structure-phase state and stress–strained state, physicochemical and mechanical properties and dispersibility of matrix components on tribotechnical characteristics of Cr–Mn–Ni alloys in the as-cast state, determining their optimal composition in terms of wear resistance.

3. Research Material and Methods

Research casts were smelted in laboratory conditions for performing researches of phase transformations and structural transformations in the solid state of chromium–manganese–nickel alloys. Charge calculation was performed on the main alloying elements for this type of alloys: C, Cr, and Mn. Chemical composition of the studied alloys is presented in Table 3 [69].

Microstructure of samples was determined in alcohol solution of nitric acid. Microstructure researches were performed with the use of 'Neophot-21' optical microscope and JSM-35 scanning electron microscope.

The number of phases and structural components in the structure of the tested alloys were determined according to the method reported in Ref. [70] at 400-fold increase. Identification of phases in the studied chromium–manganese–nickel alloys was performed according to the method of x-ray crystal analysis using DRON-3M diffractometer with the use of CuK_α-radiation. To determine the lattice parameter of unconverted austenite, the profile of refraction peaks (111)γ, (002)γ, and (113)γ were recorded on three mutually perpendicular sides of the sample (each side was recorded five times at a rate of (1/8)°/min). The lattice parameter was calculated according to the position of the mass centre of the abovementioned diffractometric maxima. The results obtained were subjected to statistical processing according to the standard method.

The amount of residual austenite was determined on the basis of the ratio of integral intensities of the lines (001) and (111) (according to the formula [71]:

$$V_\gamma = (I_{hkl\gamma}/P_{hkl\gamma})/(I_{hkl\alpha}/P_{hkl\alpha} + I_{hkl\gamma}/P_{hkl\gamma}); \quad (4)$$

here, V_γ (%) is volume ratio of austenite, $I_{hkl\gamma}$ is integral intensity of the

Table 3. **Chemical composition of chromium–manganese–nickel alloys [67]**

No.	Content of alloying elements, %									
	C	Cr	Ni	V	Mn	Si	Cu	S	P	Fe
1	2.2	12.63	0.83	0.25	5.7	1.0	0.10	0.009	0.013	77.3
2	2.7	15.91	0.95	0.25	10.5	0.9	0.9	0.009	0.027	67.9
3	3.1	13.1	1.15	0.25	15.75	0.9	0.15	0.003	0.025	65.57

line $(111)_\gamma$, $I_{hkl\alpha}$ is integral intensity of the line $(011)_\alpha$, $P_{hkl\gamma}$ is multiplicity factor for the line $(111)_\gamma$, and $P_{hkl\alpha}$ is multiplicity factor for the line $(011)_\alpha$.

Calculation of c, a parameters and the degree of tetragonality c/a of martensite was performed in the lines (211)α, $(121)_\alpha$, and $(112)_\alpha$ at $2\theta_{Fe} = 112°$ and in the lines $(020)_\alpha$, $(200)_\alpha$, and $(002)_\alpha$ at $2\theta_{Fe} = 85°$. Crystal lattice perfection level α (phases of different origin) was assessed according to the value of half-breadth ($\beta_{0.5}$) of the diffraction peak $(011)_\alpha$, determined according to the method proposed in Refs. [72, 73].

Distribution of alloying elements between the phases and structural components of chromium–manganese–nickel alloys in the as-cast state was studied using a JSM-840 electron microscope with a Link-860/500 microanalysis system (Link Analytical, England). The studies were performed according to the method of secondary-electron imaging (SEI) and backscattered electron imaging (BEI). Beam current was I = 10.7–10.9 A. Voltage was U = 20 kV. Time of analysis was t = 100 s. Beam diameter was 1–1.5 μm. The analysis was performed using the ZAF4/FLS software program. For each studied element, the clear samples were taken as standard ones (sample clearness was 99.99%). Standards provided by Link Analytical Company were used.

Microhardness of phases and structural components was determined using the PMT-3 microhardness tester according to the standard method. Hardness of chromium–manganese–nickel alloys in the as-cast state was determined by the Rockwell method. Temperature intervals of transformations were determined by means of thermal analysis on the VD-4 calorimeter when heated at a rate of 10 °C/min at the Physicotechnological Institute of Metals and Alloys of the NAS of Ukraine (Kyiv).

The impact toughness of Cr–Mn–Ni alloys was determined on samples without cutting according to GOST 9454-78 on the machine PSVO-5 with the maximum impact energy of 294 J at normal (+20 °C) and elevated (950 °C) test temperature.

The strength values of the tested alloys were calculated according to the conditions: if Brinell hardness number HB >175, $\sigma_B \approx 0.345$ HB; whereas if hardness is <175 HB, $\sigma_B \approx 0.362$ HB [65].

The method of estimating micro-fragility and fragile micro-strength [75] is based on quantitatively studied zones of fragile damage in the area of the imprint, which includes various imperfections of test material continuity caused by the influence of concentrated load (cracks, chipping). Microprinting was carried out on a PMT-3 instrument equipped with an automatic loader for the indenter, which significantly improves accuracy of the method. Imprints on the test surface were applied within a wide range of loads on the indenter (20–1000 g).

Measurements of the diagonals of the imprints d and the sizes of damage areas D were performed with an accuracy of ±0.2 μm, and the

damage area was estimated according to the maximum size of material fragile 'damage' of the material in the imprint area, no matter in which direction it occurs. Such an assessment of the damage area is most reasonable in terms of fragile strength and reliability.

Mechanical properties of carbides and austenite decomposition products were evaluated according to their microstrength (μ), microfragility (γ), and fragile microstrength (σ). The mentioned characteristics were studied depending on the depth of indenter penetration into the material, which allowed us to compare mechanical properties of material surface layers equal in their thickness.

The microfragility γ is the ratio of the plane in which fragile fracture occurs in the area of the imprint and the plane of the imprint itself. Microfragility γ of austenite decomposition products and Me_7C_3 carbide decomposition products was determined in accordance with [75]:

$$\gamma_{vd} = (D^2 - d^2)/d^2, \quad (5)$$

where D is an average size of the damaged area (μm), and d is an imprint diagonal (μm).

Fragile microstrength is the tension required to form a unit of fragile destruction in the area of the pyramid's imprint. Fragile microstrength σ_{vd} of austenite decomposition products and Me_7C_3 carbide decomposition products was determined according to the following formula [75]:

$$\sigma_{vd} = P/D^2, \quad (6)$$

where P is loads on the indenter (g), and D is defined above.

Coefficient k_{1c} was determined according to the semi-empirical Niihara dependence [76], since it is most suitable for calculation of wear resistance coefficient.

Cracking resistance k_{1c} of austenite decomposition products and Me_7C_3 carbide decomposition products was determined from the expression [77]:

$$k_{1c} = 0.203a^2H_vC^{-3/2}, \quad (7)$$

where a is a semi-diagonal of the indenter imprint (μm), H_v is the material hardness (MPa), and C is the length of the radial crack (μm).

Hardness at the Vickers pyramid indentation of the surface of the tested material was determined according to the known dependence:

$$H_v = 463.6Fa^{-2}, \quad (8)$$

where F is the load acting on the indenter (g).

Abrasion wear tests of chromium–manganese–nickel alloys in the as-cast state were carried out at normal (+20 °C) and elevated (950 °C) temperatures at the modernized friction installation 2070 SMT-1, according to the 'shaft-plane' scheme [78]. Samples in form of a parallel-

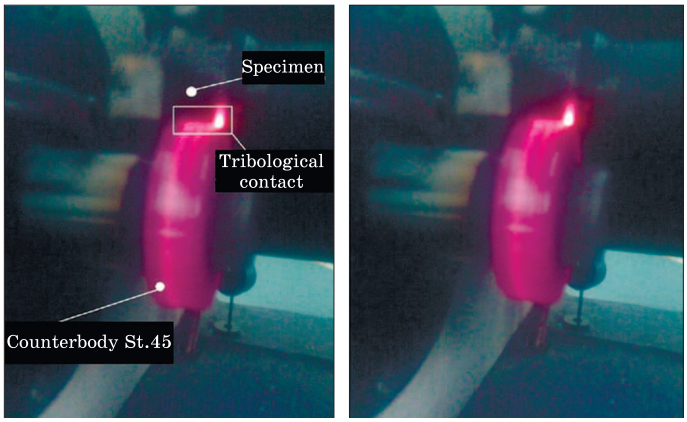

Fig. 2. Appearance of tribological contact at 1000 N load and a sliding rate of 2 m/s

epiped ($10\times10\times27$ mm^3) were used for performing tests. Steel 45 was used as the counterbody. Figure 2 shows the appearance of tribological contact at 1000 N load and a sliding rate of 2 m/s.

Currently, there are many various methods of measuring wear. They may be conditionally divided into two groups: (1) measuring changes in geometrical dimensions of the contacting surfaces and comparing the resulting values with the initial ones; (2) measuring change in mass of samples after testing. The procedure of measuring mass of samples is fairly accurate and non-labour-intensive. Only two weighings are sufficient for complete assessment of wear. However, at elevated temperatures, mechanical and chemical activation of the contact surfaces occurs. This leads to mutual transfer of materials from one surface to another, as well as increase in mass of samples due to diffusion and oxidation processes. This method can be used if the mass gain does not exceed the margin of error of the measuring instruments used. Thus, after the test, the average linear wear of the samples was measured. The frictional moment is continuously measured by means of a noncontact inductive sensor on the lower sample.

The total linear wear of samples is measured by a special meter with an inductive sensor on the upper sample. Information from frictional moment sensors and wear sensors is sent to the computer system where it is recorded, processed, and stored.

At the elevated test temperatures, the samples were mounted to a special frame, 500 N was created and they were heated by means of friction at a sliding rate of 2 m/s. Within the period of one minute, temperature at the contact reached 950 °C, (the temperature was measured by pyrometric method). Without stopping the test, the required load was set and tests were performed during five minutes, corresponding to a friction path of 600 m. Test loads were 500 N, 750 N, and 1000 N. Contact temperature at the load of 1000 N reached 1000 °C.

The time evolution process of wear consists of two unequal stages: wearing and stationary condition. The rate of wear $i_t = dI/dt$ and wear $I(t)$ as the functions of time t are of form [79]:

$$i_t(t) = (i_0 - \langle i_t \rangle)\exp(-t/T) + \langle i_t \rangle, \quad (9.1)$$

$$I(l) = (i_0 - \langle i_t \rangle)T[li_t - \exp(-t/T)] + \langle i_t \rangle t, \quad (9.2)$$

where i_0 and $\langle i_t \rangle$ are initial and average stationary value of the rate of wear, T is time of wearing in relaxation. Substituting time 't' for friction path 'l' in formulas (9.1) and (9.2), we obtain formula describing wear intensity '$I(l)$' along the friction path. Accuracy of the estimates is determined by the resolution of instruments and dispersion of the wear process.

The friction path divides the difference between six-minute wear and one-minute wear, and the value of average wear intensity (i) is obtained. During the test, the friction force is measured and the coefficient of friction (n) is calculated.

In order to determine the wear intensity, the sample should be measured before and after the test and by means of dividing by the friction path, the wear intensity in dimensionless units is obtained. Wear intensity is the ratio of wear to the friction path:

$$1\ \mu m/1\ km = 10^{-6}\ m/10^{3}\ m = 10^{-9}, \quad (10)$$

$$10\ \mu m/1\ km = 10 \cdot 10^{-6}\ m/10^{3}\ m = 10^{-8}. \quad (11)$$

Wear rate is determined in the same way by means of measuring the sample before and after the tests, and applying the ratio to the test time.

For tribological investigations, the friction installation in abrasive wear conditions was also used [80]. The scheme of this installation is presented in the Fig. 3. The tested sample (plate of 30×20 mm^2 with thickness up to 6 mm) is mounted in the holder. Sample fixation is performed with a help of clamps in the holder by means of applying the clamping force from the disk. The disk is made of rubber, its diameter is 50 mm, and its width is 15 mm.

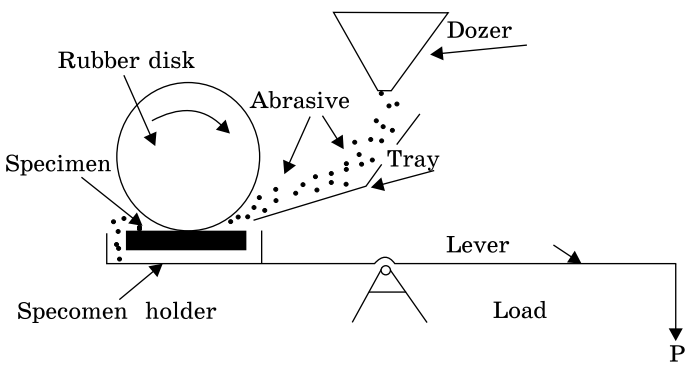

Fig. 3. Schematic diagram of the installation used for investigations in conditions of abrasive wear (win non-attached abrasive) [82]

Abrasive is in the reservoir above the disk and it enters the tray through the doser. Changing the cross-section of the doser allows providing the uniform flow of abrasive of various granularities. From the tray, the abrasive gets under the disk, which presses it to the tested sample by means of applying the force of 44.1 N. The load is regulated by means of a set of weights and the length of the lever.

Quartz sand (SiO_2) with a grain size of 500 μm, boron carbide with a grain size of 70 μm, and silicon carbide with a grain size of 180 μm were selected as the abrasives. Before testing, the samples were polished to a roughness of R_z = 0.63 μm. Surface roughness was determined on the profilometer of the 201 model. The wear was measured by weighing method with the use of electronic scales within the accuracy of 0.0001 g. Before each weighing, the samples were washed in ethyl alcohol and dried under conditions of laboratory air.

4. Cr–Mn–Ni in the As-Cast State: Structure, Phase Composition, Properties, and Distribution of Alloying Elements

This section deals with studying structure, phase composition, hardness, microhardness of structural components of Cr–Mn–Ni alloys in the as-cast state.

Microstructure of the tested samples of chromium–manganese–nickel alloys in the initial as-cast state is presented in Figs. 4 and 6. Microstructural analysis of tested samples of alloys in the as-cast state shows (Figs. 4–6) that crystallization starts with release of initial austenite dendrite and finishes with formation of eutectic colonies A + Cr_7C_3 [82, 83]. Microstructure includes Me_7C_3 carbides (both in the longitudinal section and in the cross section) and fine-differentiated austenite–carbide eutectics based on the Me_7C_3 carbide [84].

Quantitative correlations of initial austenite (A_i) and carbide eutectic (C_e) were determined by quantitative metallography and x-ray diffraction analysis. In the as-cast state for alloy No. 1, these correlations are $A_i = 65\%$, $C_e = 35\%$; for alloy No. 2, they are: $A_i = 48\%$, $C_e = 62\%$; for alloy No. 3, they are: $A_i = 22\%$, $C_e = 78\%$. Length of the plate cross sections of the Me_7C_3 eutectic carbides in all tested alloys in the as-cast state was determined. In alloy No. 1, it is 36.5 μm; for alloy No. 2, it is 42.5 μm; and in alloy No. 3, the greatest length of 55.65 μm characterizes the carbide.

Shape parameter (SP) of plates of Me_7C_3 eutectic carbides Me_7C3 in tested alloys in the as-cast state is as follows: in alloy No. 1, 3.95, in alloy No. 2, 3.85, in alloy No. 3, 2.68. Shape parameter of eutectic carbides characterizes the differentiation of the eutectic, the smaller the shape parameter, the higher the differentiation of the eutectic contributing to the strength and plastic properties of the alloy.

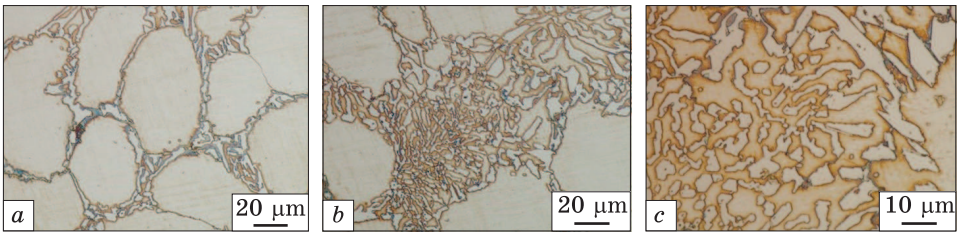

Fig. 4. Microstructure of Cr–Mn–Ni alloy in the as-cast state (alloy No. 1) with ×500 (*a*, *b*) and ×1000 (*c*) zoom factor

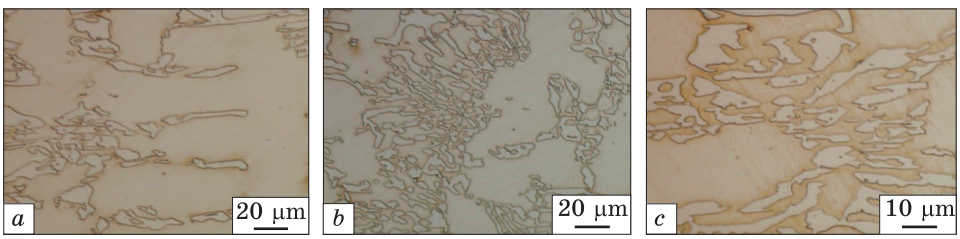

Fig. 5. The same as in the previous figure, but for alloy No. 2

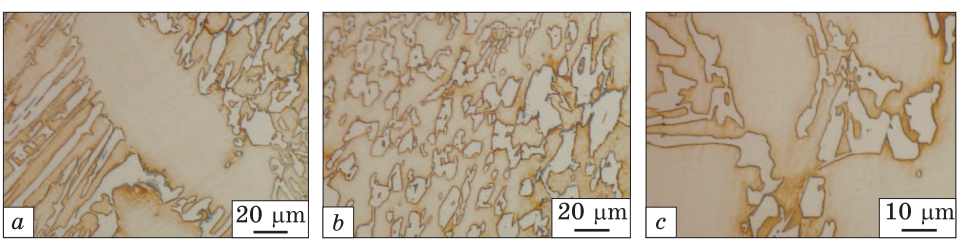

Fig. 6. The same as in the previous figure, but for alloy No. 3

Quantitative ratio of initial austenite dendrite and the eutectic component is determined by the carbon content and the ratio of the main alloying elements (chromium and manganese). In connection with this, in alloy No. 3 (where the amount of carbon and manganese is the maximal one), number of carbides is greater in comparison with alloys Nos. 1 and 2 (2.2 and 1.7 times, respectively).

The phase composition of the test chromium–manganese alloys was studied by means of x-ray diffraction analysis. Figures 7 and 8 represent diffraction pattern schemes of test chromium–manganese–nickel alloys in the as-cast state.

X-ray diffraction analysis of the tested alloys revealed [8–12] Me_7C_3 carbide (Me = Cr, Mn, Fe), cementite, austenite, and ferrite. Quantitative data of the x-ray diffraction analysis are contained in Table 4 [69].

Amount of austenite in the matrix of the tested alloys grows from 87% to 94% with increase of carbon content and content of alloying elements (Cr and Mn), and amount of ferrite decreases, respectively,

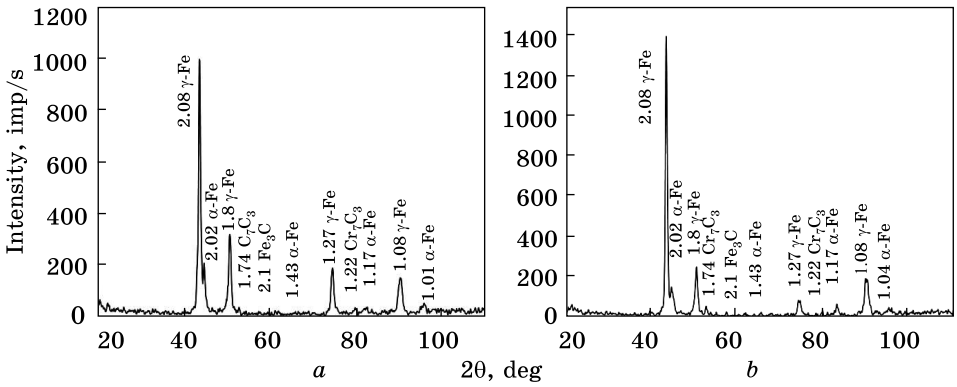

Fig. 7. Diffraction pattern schemes of Cr–Mn–Ni alloys in the as-cast state: *a* — alloy No. 1; *b* — alloy No. 2

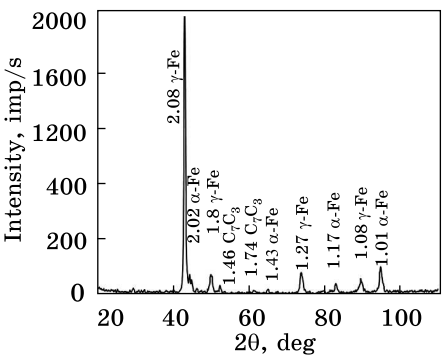

Fig. 8. The same as in the previous figure, but for alloy No. 3

from 13% to 6% (Table 4). The presence of ferrite is probably due to insufficient stability of austenite, which undergoes decomposition into ferrite and carbide in the process of cooling.

Analysis of data in Table 4 shows that the structure of sparingly alloyed allays contains practically balanced α-phase with the degree of lattice imperfection ($\beta_{0.5}$) in the range from 0.57 to 0.59, the lattice parameter of α-phase (a_α) fluctuates within the range of 2.87–2.88.

Microhardness of phases and structural components of the tested alloys in the as-cast state are presented in Table 5 [69]. Matrix microhardness and microhardness of eutectic carbides in all tested alloys increase with increasing amounts of carbon, chromium, and manganese (Table 5).

Table 6 presents mechanical properties of chromium–manganese–nickel alloys in the as-cast state. Analysis of the obtained data shows that with increasing content of carbon and manganese content hardness

Table 4. **Quantitative data of x-ray diffraction analysis of Cr–Mn–Ni alloys in the as-cast state [69]**

No.	a_α to $(011)_\alpha$	a_γ to $(022)_\gamma$	Degree of imperfection of α-phases ($\beta_{0.5}$)	% γ, in the matrix	% α, in the matrix
1	2.87	3.60	0.59	87	13
2	2.88	3.62	0.59	92	8
3	2.87	3.62	0.57	94	6

of the tested alloys in the as-cast state increases by 25% and their strength limit is increased by 24%. Hardness of alloys Nos. 2 and 3 is the same (42 HRC units), and hardness of alloy No. 1 is much lower (35 HRC units) as Table 6 indicates.

Table 7 shows the impact toughness of chromium–manganese–nickel alloys in the as-cast state at room temperature and at elevated test temperatures. Impact toughness of tested alloys in the as-cast state at the test temperature of 20 °C is the same, namely, 5.9 J/cm^2. Heating up to 950 °C leads to increase of impact toughness: in alloy sample No. 1, it rises 2.6 times; in the sample No. 2, it rises 1.3 times; whereas the hardness of alloy No. 3 does not change.

Tables 8 and 9 demonstrate micromechanical characteristics of carbides and matrices in Cr–Mn–Ni alloys in the as-cast state. Microhardness of matrix, eutectic carbides and micromechanical characteristics matrices and eutectic carbides of all tested alloys in the as-cast state increase with increasing amount of carbon, Cr and Mn (Tables 8 and 9).

Thus, the maximal strength and hardness in the as-cast state are typical for alloy samples Nos. 2 and 3, and this gives an opportunity to predict the increase of abrasive wear resistance and impact-abrasive wear resistance and wear resistance in conditions of friction at high temperatures and loads in the as-cast state and heat-treated state. The indicated difference in properties of chromium–manganese–nickel alloys is determined by distribution of alloying elements between phases and structural components in the test Cr–Mn–Ni alloys, and namely by the degree of alloying the matrix and eutectic carbide, as well as by the shape parameter of the eutectic carbide.

Table 5. **Microhardness of phases and structural components of testable Cr–Mn–Ni alloys in the as-cast state [69]**

No.	Microhardness of structural components, MPa		
	A–K eutectic	Matrix	Eutectic carbide
1	7920	4137	6577
2	8934	4228	8244
3	9195	4663	8965

Table 6. **Mechanical properties of Cr–Mn–Ni alloys in the as-cast state [85, 86]**

No.	Hardness, HRC	Strength limit $\sigma_в$, MPa
1	35	111
2	42	138
3	42	138

Table 7. **Impact toughness of Cr–Mn–Ni alloys in the as-cast state at room and elevated temperatures [85, 86]**

No.	Test temperature, °C	Impact toughness, J/cm^2
1	20	5.9
	950	15.6
2	20	5.9
	950	7.8
3	20	5.9
	950	5.9

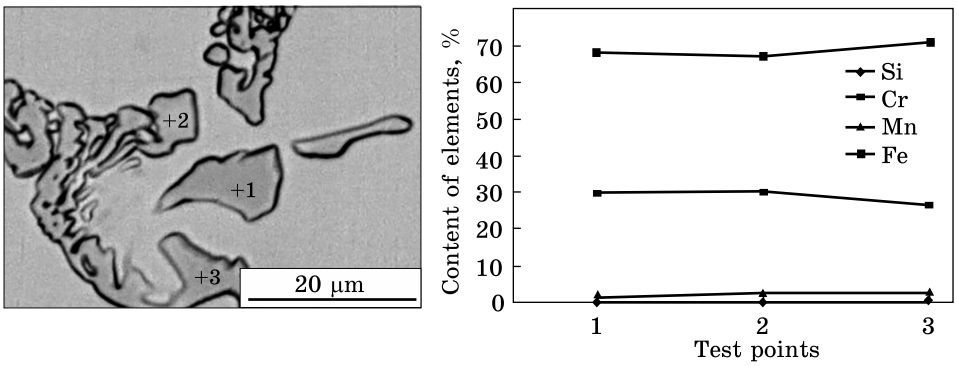

Fig. 9. Distribution of alloying elements (Si, Cr, Mn, Fe) among the phases and structural components of the Cr–Mn–Ni alloy in the as-cast state (alloy No. 1)

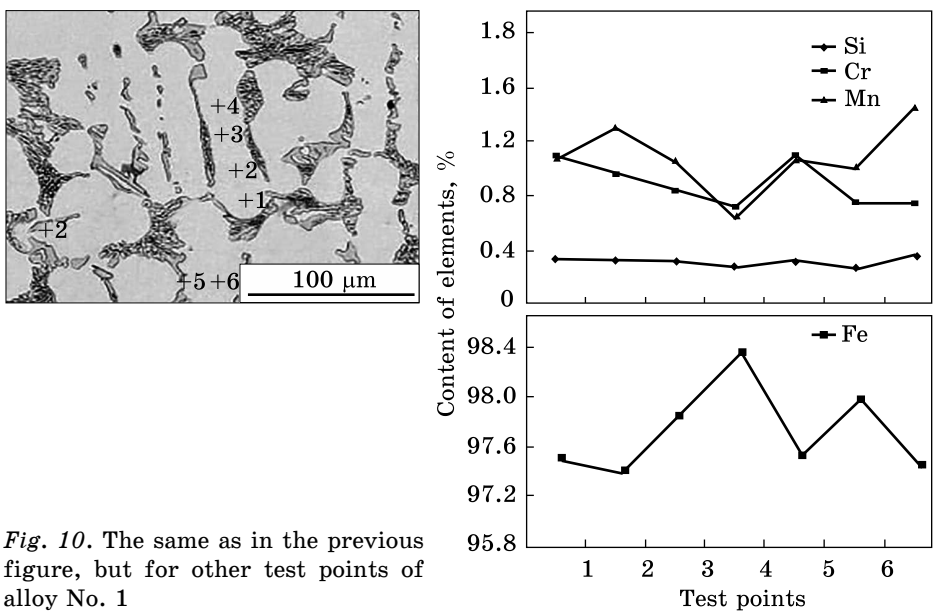

Fig. 10. The same as in the previous figure, but for other test points of alloy No. 1

The distribution of alloying elements between the phases and the structural components in the tested chromium–manganese–nickel alloys in the as-cast state was studied by means of local x-ray spectral analysis. Quantitative local x-ray spectral analysis of samples made of Cr–Mn–Ni alloys was performed pointwise; content of alloying elements in the matrix and carbides was analysed. Results of tests are presented in Figs 9–14. Quantitative data are given in Tables 10–12.

Applying the local x-ray spectral analysis, it was determined that in the tested alloys in eutectic carbide chromium is present in quantities of ≈34.9–36.7%, amount of manganese is 8.9–9.33%, and percentage of silicon is 0.11–0.23%. Results of local x-ray spectral analysis on dis-

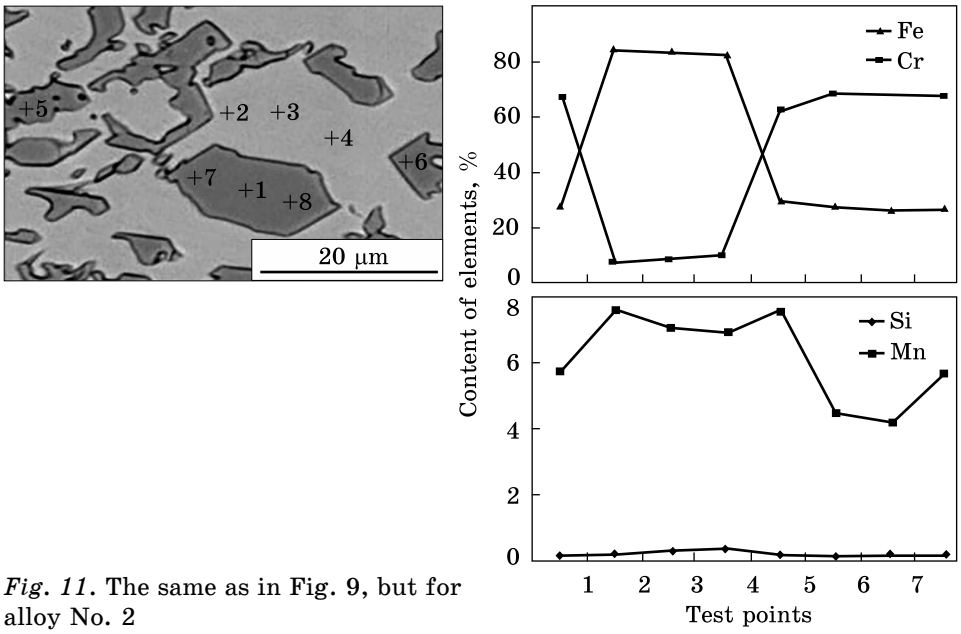

Fig. 11. The same as in Fig. 9, but for alloy No. 2

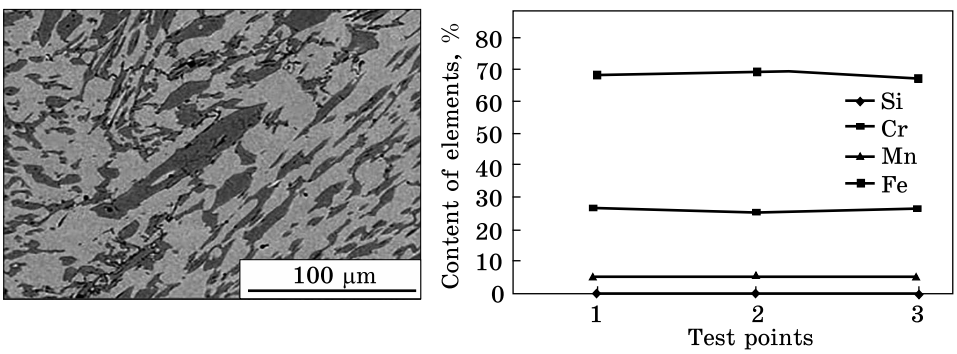

Fig. 12. The same as in the previous figure, but for other test points of alloy No. 2

tribution of alloying elements between phases and structural components indicate that with increase of C, Cr, and Mn in the tested alloys, the degree of alloying the matrix and eutectic carbide increases, which ensures increased microhardness, hardness, and, respectively, improved wear resistance.

5. Bainitic Nanostructured Matrix Formation in Cr–Mn–Ni

Nowadays, the properties of castings made of sparingly alloyed high-chromium and Cr–Mn–Ni alloys, operating under conditions of intensive abrasive wear, impact-abrasive wear, corrosion wear, erosion wear,

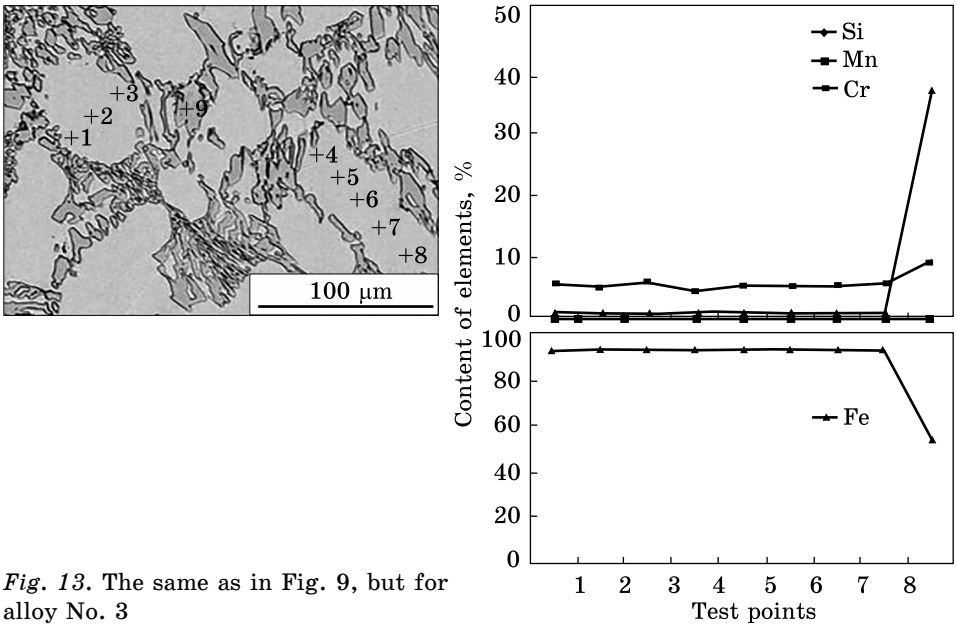

Fig. 13. The same as in Fig. 9, but for alloy No. 3

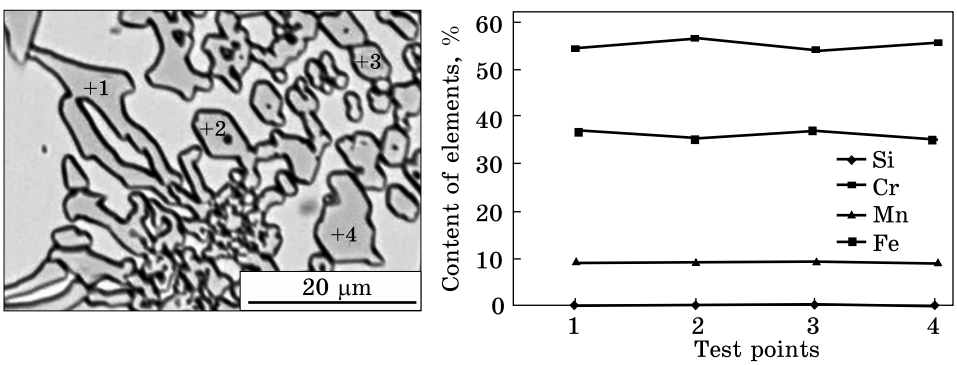

Fig. 14. The same as in the previous figure, but for other test points of alloy No. 3

as well as friction wear at high temperatures and loads can be significantly improved by means of isothermal hardening due to isothermal bainitic hardening in the solid state. For further developing regimes of isothermal hardening giving an opportunity to improve service life of parts used in metallurgical equipment and machine-building equipment, it is necessary to research regularities of forming bainitic nanostructural matrix as well as kinetics of phase transformations in the bainitic range of temperatures in Cr–Mn–Ni alloys.

The regularities of structure formation and kinetics of phase transformations in the tested alloys were studied by means of the dilatomet-

Table 8. **Micromechanical characteristics of carbides in the as-cast Cr–Mn–Ni alloys [85, 86] (see Eqs. (5)–(8))**

No.	Microhardness of Me_7C_3 carbide, MPa	Microfragility of Me_7C_3 carbide (γ), relative units	Fragile microstrength of Me_7C_3 carbide (σ_{vd}), kgf/mm^2	Cracking resistance of Me_7C_3 carbide (k_{1c}), MPa·m$^{1/2}$
1	6577	5.5	3.33	4.49
2	8244	6.89	3.74	4.37
3	8965	7.49	6.41	3.92

Table 9. **Micromechanical characteristics of matrices in Cr–Mn–Ni alloys in the as-cast state [85, 86]**

No.	Matrix microhardness, MPa	Matrix microfragility γ, relative units	Fragile microstrength of matrix (σ_{vd})	Matrix cracking resistance (k_{1c})
1	4137	1.03	1.59	7.23
2	4228	1.98	1.87	7.15
3	4663	1.16	1.96	8.83

Table 10. **Quantitative data of distribution of alloying elements among the phases and structural components of the Cr–Mn–Ni alloy in the as-cast state (alloy No. 1)**

Structural components	Content of alloying elements in the structural components, %				
	Cr	Mn	Si	Fe	Sum of alloying elements, %
Matrix	1.09	1.04	0.33	97.54	2.46
Cr_7C_3 carbide	34.9	8.9	0.11	56.09	43.91

Table 11. **The same as in the previous table, but for alloy No. 2**

Structural components	Content of alloying elements in structural components, %				
	Cr	Mn	Si	Fe	Sum of alloying elements, %
Matrix	8.28	6.88	0.27	84.57	15.43
Cr_7C_3 carbide	36.7	9.33	0.23	53.74	46.26

Table 12. **The same as in the previous table, but for alloy No. 3**

Structural components	Content of alloying elements in structural components, %				
	Cr	Mn	Si	Fe	Sum of alloying elements, %
Matrix	5.27	5.3	0.26	89.17	10.83
Cr_7C_3 carbide	35.8	9.2	0.21	54.79	45.21

ric method in the temperature range of 500–150 °C. Samples were kept in a dilatometer for up to 40 h at predetermined temperatures, and then the structure was fixed by means of sample hardening. The bends on the curves indicate presence of phase transformations in the alloy.

Figures 15–17 show dilatograms of tested Cr–Mn–Ni alloys with various contents of Mn, Cr, and Ni. Based on the obtained data, the isothermal decomposition diagrams of the supercooled austenite for tested Cr–Mn–Ni alloys were formed.

Figures 18–20 show the decomposition diagrams of supercooled austenite for tested alloys. Diagram of alloy sample No. 1 (Fig. 18) is characterized by separation of transformation temperature intervals. The minimum resistance of austenite is observed at a temperature of 400 °C. Decomposition of austenite starts after soaking for a period of 20 h and lasts until the end of soaking during 24 h. During this process, a significant amount of residual austenite (81%) is preserved in the structure. Zone of high resistance of initial austenite is in the temperature range of 350–300 °C. When held within this temperature range, cast iron is not subjected to transformations, but an insignificant release of secondary carbides can be observed (Fig. 21).

The second supercooled austenite transformation area is within the temperature range of 250–200 °C. This transformation starts at a temperature of 250 °C after soaking for 21.5 h; the ratio of residual austenite after soaking within this temperature range is ≈83%. In this case, the transformation of austenite is more intense at a temperature of 200 °C, as evidenced by presence of austenite decomposition products in the structure, as well as by the ratio of residual austenite at the level of ≈78%.

Figure 22 shows microstructure of chromium–manganese–nickel alloy No. 1 after isothermal soakings in the temperature range of 250–200 °C. It should be noted that the transformation of supercooled austenite takes place to a small extent in both zones, a high amount of residual austenite remains in the structure of the tested samples.

The obtained data correlate well with the data of x-ray diffraction analysis. Figure 23 shows microstructure of the tested alloy after isothermal soakings in the temperature range of 400–200 °C. Analysis of diffraction patterns of Cr–Mn–Ni alloy subjected to isothermal treatment indicates presence of ferrite, Me_7C_3 (Me = Cr, Mn, Fe) eutectic carbides, alloyed cementite and residual austenite in the structure.

Table 13 shows data of x-ray diffraction analysis of samples of Cr–Mn–Ni alloy No. 1 in the as-cast state and subjected to the isothermal processing. Isothermal soaking at a temperature of 400 °C leads to the fact that the structure of Cr–Mn–Ni alloy No. 1 attains α-phase with the degree of lattice imperfection ($\beta_{0.5}$) of 0.5°, the lattice parameter of α-phase (a_α) is 0.287 nm. At the same time, the amount of residual austenite is ≈81%.

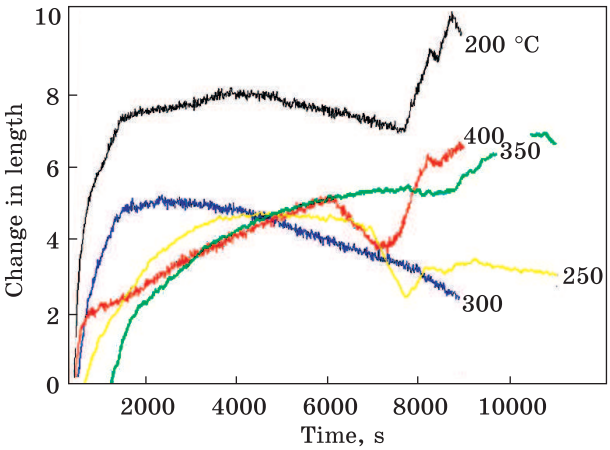

Fig. 15. Dilatograms of the tested Cr–Mn–Ni alloy (No. 1)

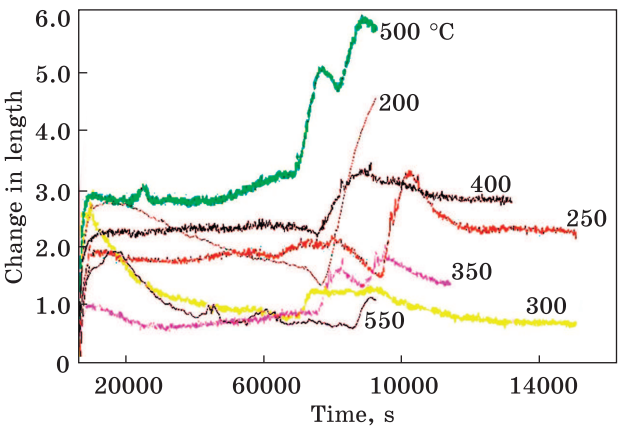

Fig. 16. The same as in the previous figure, but for alloy No. 2

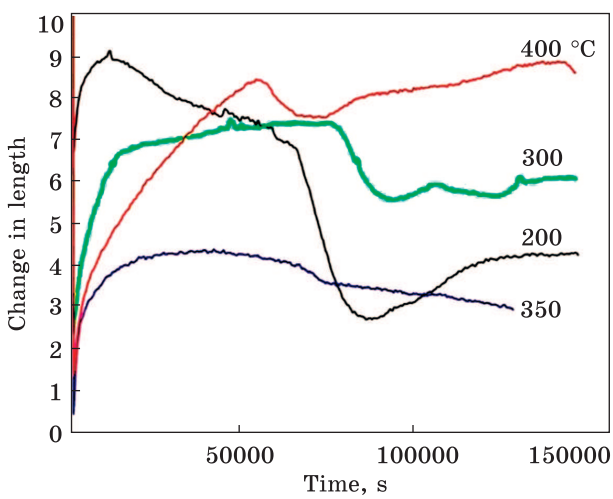

Fig. 17. The same as in Fig. 15, but for alloy No. 3

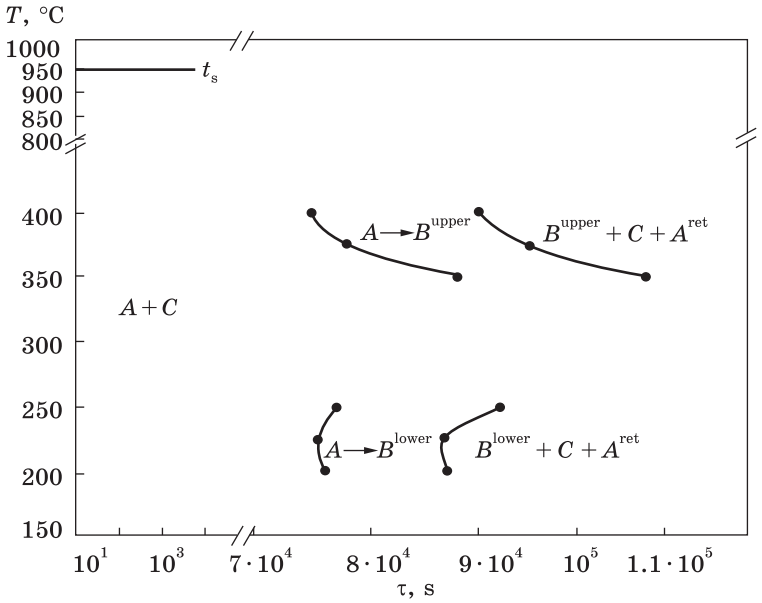

Fig. 18. Isothermal decomposition diagram of supercooled austenite of the tested Cr–Mn–Ni (alloy No. 1), where, *A*, *B*, and *C* denote austenite, bainite, and cementite, respectively

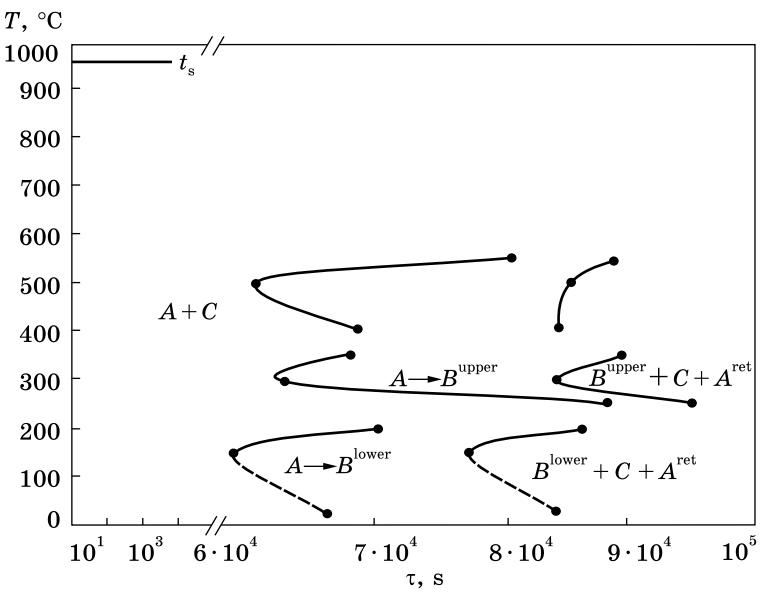

Fig. 19. The same as in the previous figure, but for alloy No. 2 [87]

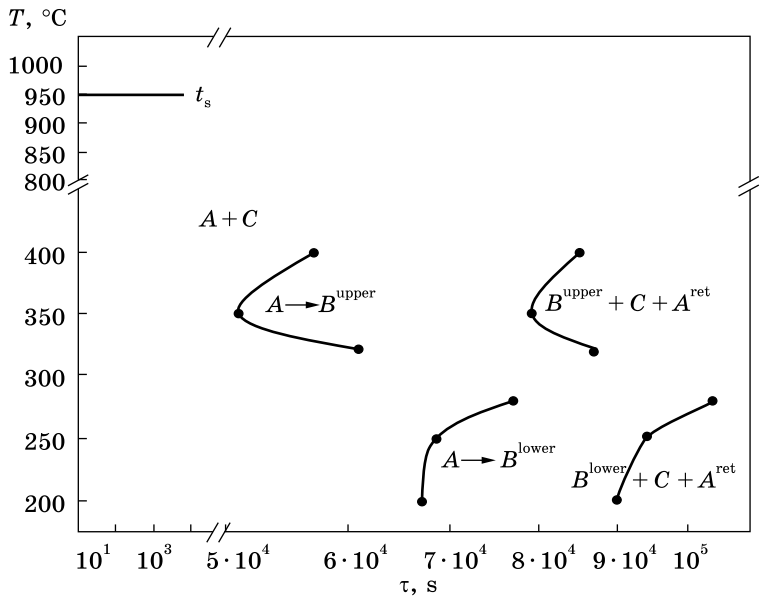

Fig. 20. The same as in Fig. 18, but for alloy No. 3

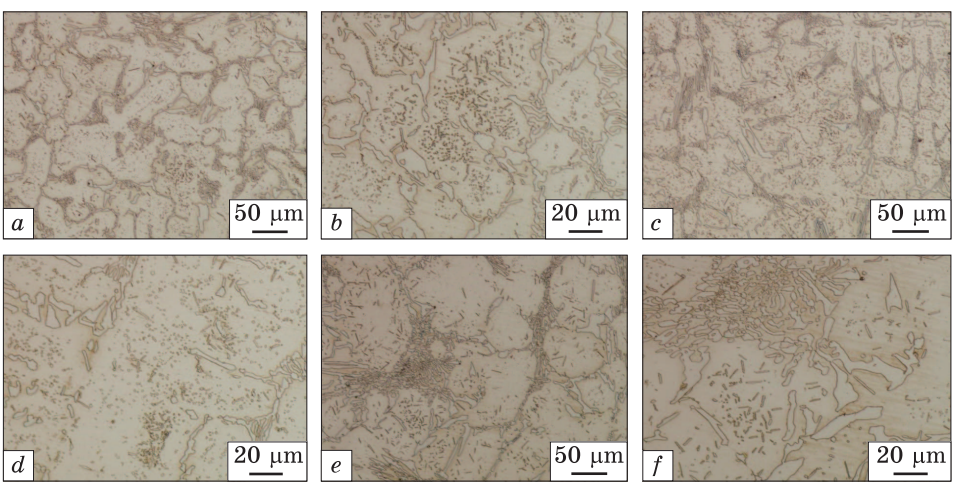

Fig. 21. Microstructure of Cr–Mn–Ni (alloy No. 1) after isothermal soakings: T = = 400 °C, soaking time τ = 24 h (*a*, *b*); T = 350 °C, τ = 30 h (*c*, *d*); T = 300 °C, τ = = 24 h (*e*, *f*). Zoom factors: ×200 (*a*, *c*, *e*) and ×500 (*b*, *d*, *f*)

After soaking at a temperature of 350–300 °C, the structure retains a large amount of unconverted austenite (86%), which indicates the presence of a 'time window' at this temperature. Decrease in the temperature of isothermal soaking down to 250 °C leads to a decrease of the amount of residual austenite in the structure of the tested samples down to 83%.

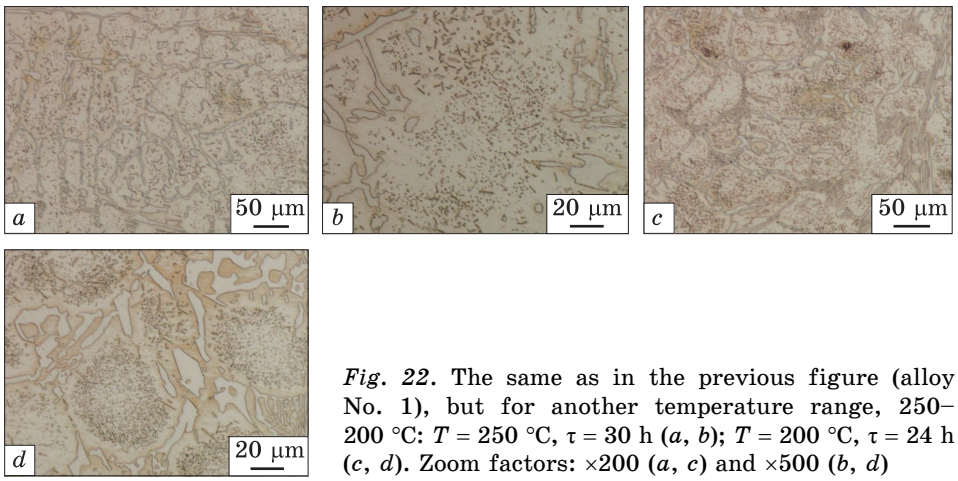

Fig. 22. The same as in the previous figure (alloy No. 1), but for another temperature range, 250–200 °C: T = 250 °C, τ = 30 h (*a*, *b*); T = 200 °C, τ = 24 h (*c*, *d*). Zoom factors: ×200 (*a*, *c*) and ×500 (*b*, *d*)

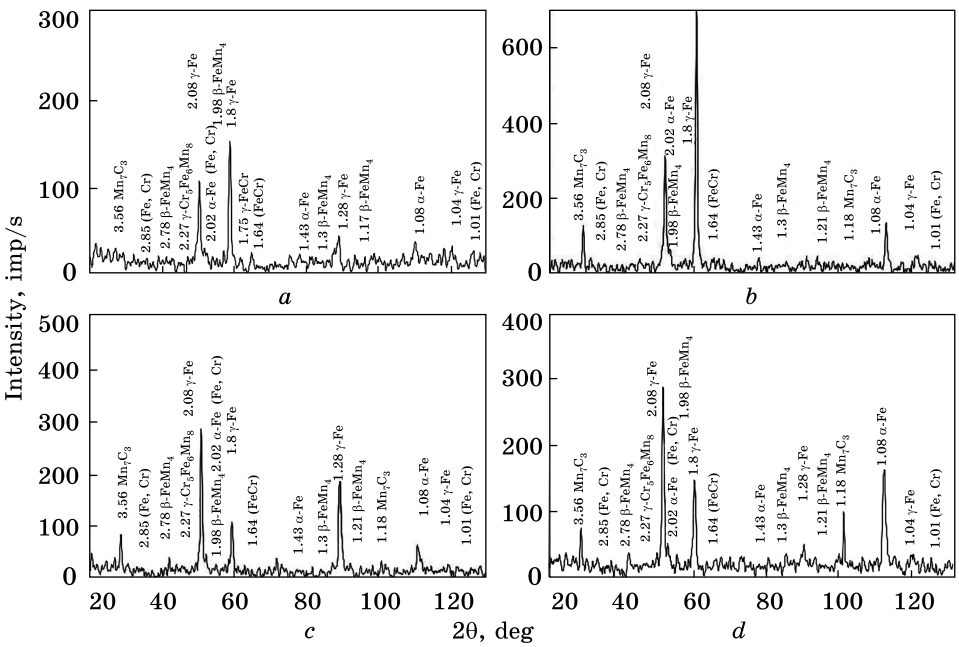

Fig. 23. Diffraction patterns of Cr–Mn–Ni (alloy No. 1) after isothermal soakings within the temperature range 400–200 °C: T = 400 °C, τ = 24 h (*a*); T = 350 °C, τ = = 30 h (*b*); T = 250 °C, τ = 24 h (*c*); T = 200 °C, τ = 30 h (*d*)

After soaking at a temperature of 200 °C, a decrease of the degree of lattice imperfection ($\beta_{0.5}$) is observed (0.44), the amount of residual austenite is ≈78%.

Diagram of alloy No. 2 (Fig. 19) is characterized by separation of transformation temperature intervals as well as by high resistance of

the austenite region due to an increased contents of Mn. Resistance of supercooled austenite below A_{c3} temperature depends on the temperature of isothermal soaking. The minimum resistance of austenite in the region of pearlite transformation is observed at a temperature of 500 °C. Decomposition of austenite starts after soaking for a period of 19 h and finishes only upon expiration of 24 h. During this process, a small amount of residual austenite (15%) is preserved in the structure. Isothermal soaking at a temperature of 550 °C leads to a significant increase of austenite resistance. In this case, the decomposition of austenite into pearlite begins after 23.5 h, and after fixing the structure (after 24 h) the amount of residual austenite is 28%.

In the temperature range of 400–350 °C, an area of austenite high resistance (the so-called 'time window'). However, only a small amount of austenite undergoes transformation, after soaking for 35 h the share of unconverted austenite is ≈88%.

Figure 24 shows microstructure of Cr–Mn–Ni alloy No. 2 after isothermal soakings in the temperature range of 550–400 °C. The structure presented in Fig. 24 confirms the presence of pearlitic transformation area in the diagram. Transformation begins to develop on the boundaries of austenite dendrites, as evidenced by the accumulation of secondary carbides and their location around the pearlite colonies, whereas in the centre of the dendrites, the number of carbides is much smaller. In the temperature range 400–350 °C, the area of pearlitic and bainitic transformation is observed, which is characterized by a high austenite resistance.

Figures 24, *e*, *f* illustrate microstructures corresponding to the area of austenite maximal resistance. In this area, austenite retains stability for up to 21 h and only 5% of austenite undergoes transformation, and the change in sample length in this area is probably due to release and arrangement of secondary carbides within the dendrites in form of chains.

In the intermediate temperature range of 350–250 °C, the minimal resistance of austenite is observed at a temperature of 300 °C. Decom-

Table 13. **Quantitative data of x-ray diffraction analysis of the samples of Cr–Mn–Ni alloy No. 1 in the as-cast state and after isothermal soakings**

State of tested specimens	a_α to $(011)_\alpha$, nm	a_γ to $(022)_\gamma$, nm	Degree of imperfection of α-phase ($\beta_{0.5}$), deg.	% γ
as-cast state	0.287	0.36	0.59	87
$T_{isothermal}$ = 400 °C, soaking time τ = 24 h	0.287	0.359	0.5	81
$T_{isothermal}$ = 350 °C, τ = 30 h	0.22	0.359	0.52	87
$T_{isothermal}$ = 300 °C, τ = 24 h	0.23	0.359	0.42	86
$T_{isothermal}$ = 250 °C, τ = 30 h	0.24	0.36	0.551	83
$T_{isothermal}$ = 200 °C, τ = 24 h	0.24	0.359	0.44	78

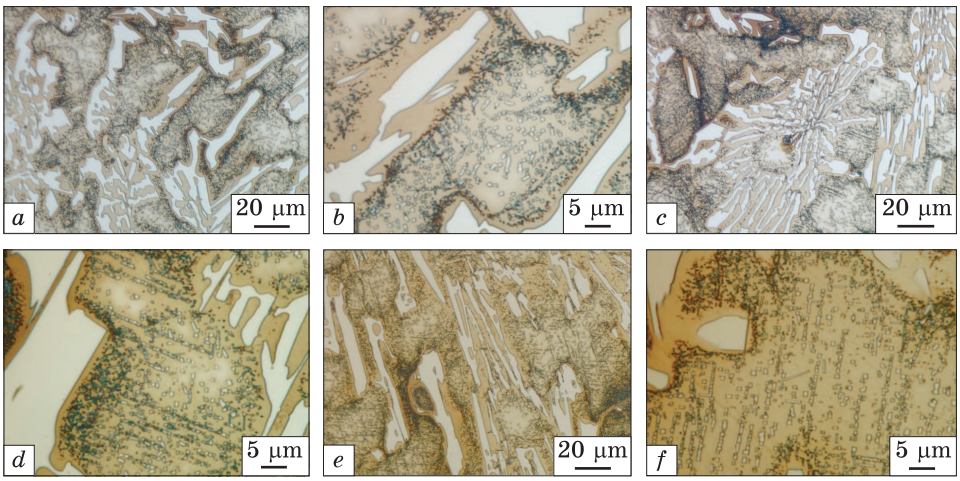

Fig. 24. Microstructures of Cr–Mn–Ni (alloy No. 2) after isothermal soakings: T = 550 °C, τ = 24 h (*a*, *b*); T = 500 °C, τ = 24 h (*c*, *d*); T = 400 °C, τ = 35 h (*e*, *f*) [87]. Zoom factors: ×500 (*a*, *c*, *e*), ×1500 (*b*, *d*, *f*)

position of austenite starts after soaking for a period of 19.5 h and finishes only upon expiration of 27 h. However, the transformation is not complete; the structure retains a large amount of residual austenite (≈53%). Increase in the temperature of isothermal soaking up to 350 °C leads to an increase in the austenite resistance. In this case, the decomposition of austenite with the formation of bainite begins after 20.5 h and finishes after 28 h. An absence of bends on the dilatograms in the process of further soaking for up to 30 h also indicates an absence of further transformations, with the amount of residual austenite remaining at the level of ≈50%.

Resistance of supercooled austenite increases sharply as the isothermal decomposition temperature drops down to 250 °C. In this case, the first bainitic colonies appear only after 26 h. In the process of further soaking during a period of up to 40 h, only 23–26% of supercooled austenite undergoes decomposition. As the structure retains a large amount of austenite (≈66%), it can be assumed that there is one more area of austenite high resistance in the 250–210 °C temperature range. Since, at high content of Mn in cast iron, the onset temperature of martensitic transformation lies in the region of negative temperatures, then, at a room temperature cooling, the residual austenite is also retained in the structure.

Figure 25 shows the microstructure of Cr–Mn–Ni alloy No. 2 after isothermal soakings in the temperature range of 350–250 °C. Bainitic type microstructures that cannot be interpreted in optical metallographic researches are presented [88–91].

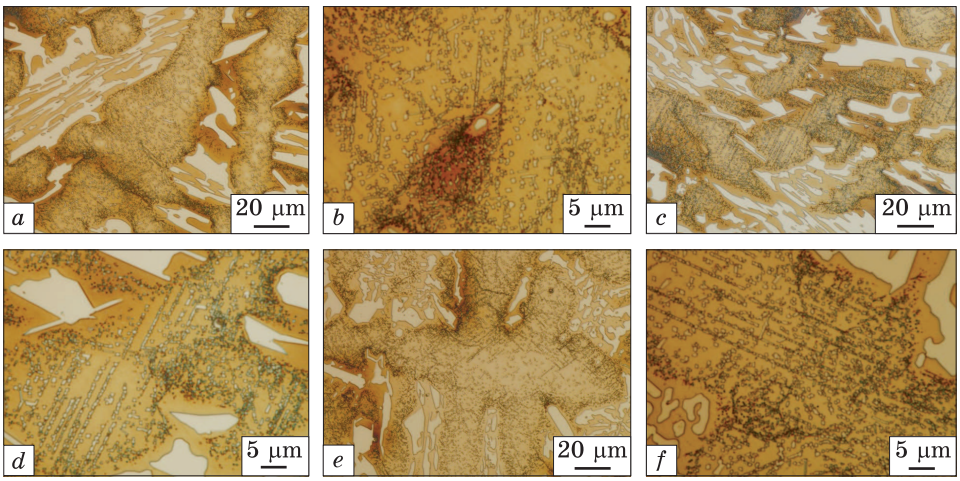

Fig. 25. The same as in the previous figure (alloy No. 2), but for T = 350 °C, τ = 30 h (*a*, *b*); T = 300 °C, τ = 40 h (*c*, *d*); T = 250 °C, τ = 40 h (*e*, *f*) [87]

After isothermal soaking at the temperatures of 350–250 °C, the eutectic carbides and secondary carbides are observed in the microstructure of the samples; bainite and residual austenite are present in the matrix. The typical arrangement of secondary carbides in form of chains is presented in Figs. 25, *b*, *d* and *f* can probably be explained by the presence of bainite in the structure. As a result, carbides are arranged along the ferrite plates. Secondary cross sections of carbides have the most variable shapes: round, rhombic, and hexagonal.

Figure 26 shows diffractograms of Cr–Mn–Ni alloy (alloy No. 2) after isothermal soakings at the temperatures of 550–250 °C. The analysis of the diffraction patterns of the alloy after isothermal treatment indicates that the structure contains ferrite, $(Cr,Mn,Fe)_7C_3$ eutectic along with $(Cr,Mn,Fe)_2C$ and $(Cr,Mn,Fe)_5C_2$ secondary carbides, doped cementite, and residual austenite.

For comparison, Table 14 shows the x-ray diffraction analysis data for samples of Cr–Mn–Ni alloy No. 2 in the as-cast state and after being subjected to the isothermal processing. The value of $\beta_{0.5}$ line $(011)_\alpha$ characterizing imperfection level of α-phase presented in the alloy in form of eutectoid ferrite, bainitic ferrite; amount of non-decomposed residual austenite (γ, %); residual austenite parameter (a_γ) and parameter of α-phase (a_α).

The analysis of data presented in Table 14 shows that isothermal soaking at a temperature of T = 550 °C leads to the fact that the structure of chromium–manganese–nickel alloy No. 2 becomes α-phase with a small degree of lattice imperfection ($\beta_{0.5}$) equal to 0.29°, the lattice parameter of α-phase (a_α) is 0.287 nm. At the same time, the amount of

residual austenite is ≈28%. At a temperature of 500 °C corresponding to the minimal resistance of austenite in the pearlite area (19 h), a decrease in the degree of lattice imperfection ($\beta_{0.5}$) is observed (0.19) alongside with a decrease of residual austenite amount (≈16%). After soaking at a temperature of 400 °C, the structure retained a large amount of unconverted austenite (88%), which indicates the presence of a 'time window' at this temperature.

Isothermal soaking at a temperature of 350 °C leads to the fact that the structure of the test cast iron includes α-phase with a small degree of lattice imperfection ($\beta_{0.5}$) equal to 0.2°; the lattice parameter of α-phase (a_α) is 0.288 nm. Amount of unconverted austenite remains at a high level (≈50%). At a temperature of 300 °C corresponding to the minimal resistance of austenite in the bainitic area (19.5 h), the level of lattice imperfection ($\beta_{0.5}$) is 0.21°, lattice parameter of α-phase does not change (a_α) (0.288 nm), and amount of residual austenite remains at the level of ≈53% even with soaking time of 40 h. After soaking at a temperature of 250 °C, the structure retained a large amount of untransformed austenite (≈66%). At a temperature of 200 °C, a decrease in the degree of lattice imperfection ($\beta_{0.5}$) is observed (0.23), and the amount of residual austenite is ≈16%. Quantitative data presented in Table 14 indicate that in the process of long-term soakings the ferrite component of bainite undergoes drawing back and in the result of this, values of α-phase lattice parameter are close to equilibrium values.

Table 15 presents measured microhardness values of austenite decomposition products and eutectic carbides as well as hardness values of chromium–manganese–nickel alloy No. 2 in the as-cast state and after isothermal soakings.

Analysis of hardness values of chromium–manganese–nickel alloy shows that there is a satisfactory correlation between the data of metal-

Table 14. **The same as in the previous table, but for alloy No. 2 [87]**

State of tested samples	a_α by (011)α, nm	a_γ by (022)γ, nm	Degree of imperfection of α-phase ($\beta_{0.5}$), deg.	% γ
as-cast state	0.288	0.362	0.59	92
$T_{\text{isothermal}}$ = 550 °C, τ = 24 h	0.287	0.361	0.29	28
$T_{\text{isothermal}}$ = 500 °C, τ = 24 h	0.287	0.375	0.19	16
$T_{\text{isothermal}}$ = 400 °C, τ = 35 h	0.288	0.376	0.16	88
$T_{\text{isothermal}}$ = 350 °C, τ = 30 h	0.289	0.377	0.2	50
$T_{\text{isothermal}}$ = 300 °C, τ = 40 h	0.288	0.377	0.21	53
$T_{\text{isothermal}}$ = 250 °C, τ = 40 h	0.288	0.377	0.2	66
$T_{\text{isothermal}}$ = 200 °C, τ = 24 h	0.287	0.360	0.23	16
$T_{\text{isothermal}}$ = 150 °C, τ = 35 h	0.288	0.360	0.37	82
$T_{\text{isothermal}}$ = 25 °C, τ = 35 h	0.288	0.360	0.29	76

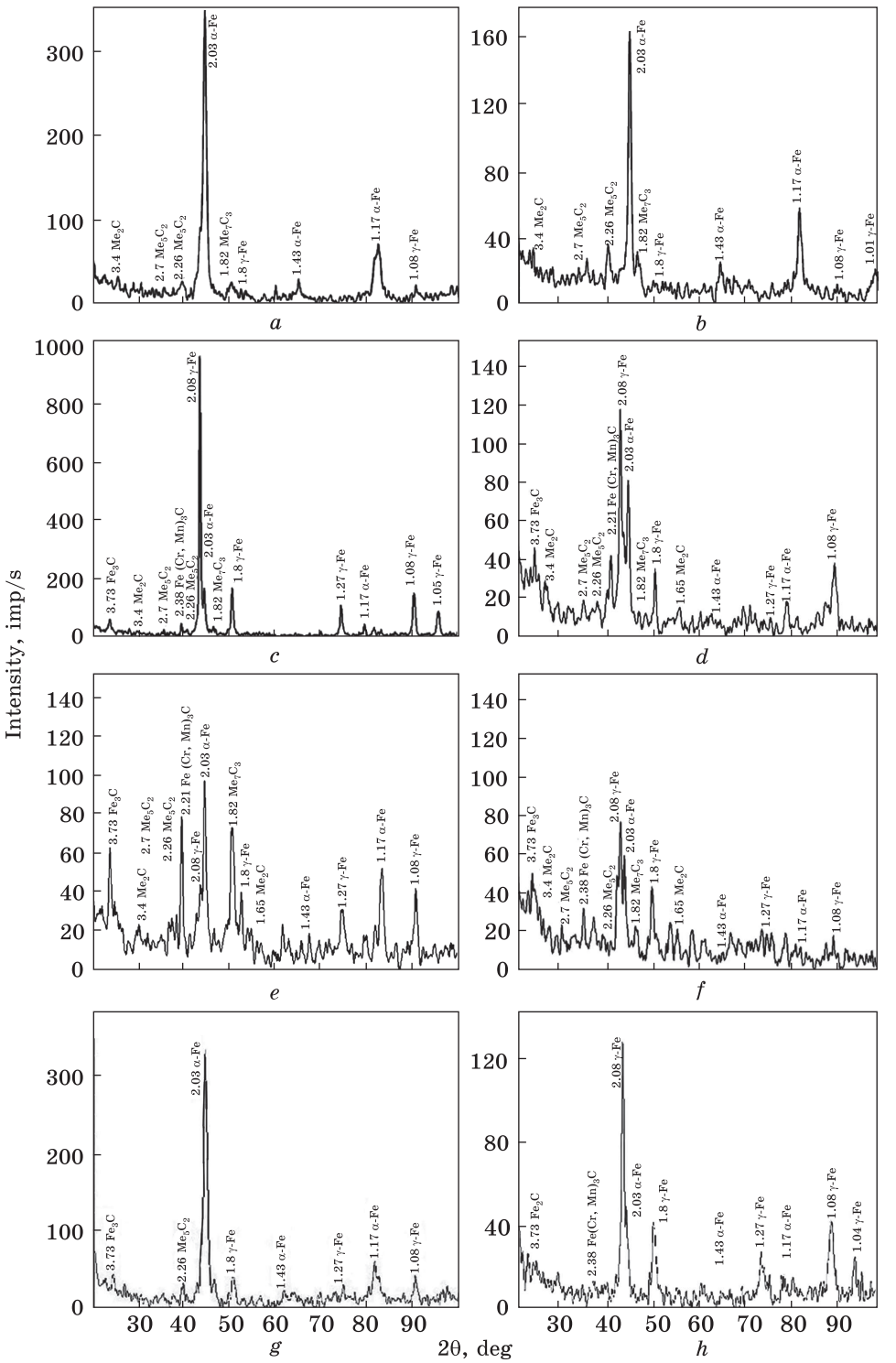
Intensity, imp/s
2θ, deg
a
b
c
d
e
f
g
h
3.4 Me3C
2.7 Me3C2
2.26 Me3C2
2.03 α-Fe
1.82 Me7C3
1.8 γ-Fe
1.43 α-Fe
1.17 α-Fe
1.08 γ-Fe
1.01 γ-Fe
3.73 Fe3C
2.38 Fe (Cr, Mn)3C
2.08 γ-Fe
1.27 γ-Fe
1.05 γ-Fe
2.21 Fe (Cr, Mn)3C
1.65 Me2C
1.04 γ-Fe

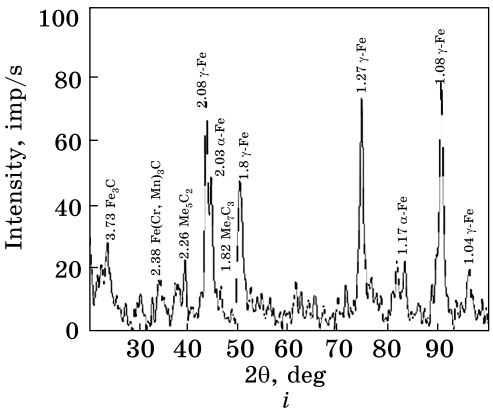

Fig. 26. Diffractograms of Cr–Mn–Ni (alloy No. 2) for isothermal soakings: T = 550 °C, τ = 24 h (*a*); T = = 500 °C, τ = 24 h (*b*); T = 400 °C, τ = = 35 h (*c*); T = 350 °C, τ = 30 h (*d*); T = 300 °C, τ = 40 h (*e*); T = 250 °C, τ = 40 h (*f*); T = 200 °C, τ = 24 h (*g*); T = 150 °C, τ = 35 h (*h*); T = 25 °C, τ = 35 h (*i*) [87]

lographic x-ray refraction tests and change of hardness during heat treatment of the tested alloy. The maximal hardness is typical for the alloy after isothermal soaking in the pearlite temperature range $T_{\text{isothermal}}$ = 500 °C, during 24 h (46.7 HRC) and in the intermediate temperature range at $T_{\text{isothermal}}$ = 250 °C during 40 h (49 HRC).

The maximum microhardness of austenite decomposition products and eutectic colonies is ensured by means of isothermal soakings of the tested alloy No. 2 at 500 and 250 °C.

Dilatometric tests of the chromium–manganese–nickel alloy No. 3 show that in the process of isothermal soakings (Fig. 17) at 400 °C turns on the curve indicate presence of austenite–ferrite phase transformation. The transformation begins after 15.5 h, and according to the x-ray analysis, the ratio of residual austenite is ≈71%. Dilatograms (Fig. 17) recorded during isothermal soakings at 300 °C and 200 °C show a similar

Table 15. **Microhardness values of austenite decomposition products and eutectic carbides. Hardness values of Cr–Mn–Ni alloy No. 2 in the as-cast state and after isothermal soakings [87]**

State of tested specimens	Microhardness of structural components (H_μ), MPa		Hardness, HRC
	A–*K* eutectic	Matrix	
as-cast state	5610	3520	42
$T_{\text{isothermal}}$ = 550 °C, τ = 24 h	4953	4226	46.2
$T_{\text{isothermal}}$ = 500 °C, τ = 24 h	4729	4213	46.7
$T_{\text{isothermal}}$ = 400 °C, τ = 35 h	4685	4366	45.1
$T_{\text{isothermal}}$ = 350 °C, τ = 30 h	4631	4451	45
$T_{\text{isothermal}}$ = 300 °C, τ = 40 h	4642	4140	45.5
$T_{\text{isothermal}}$ = 250 °C, τ = 40 h	6438	4290	49
$T_{\text{isothermal}}$ = 200 °C, τ = 24 h	4805	4154	45.6
$T_{\text{isothermal}}$ = 150 °C, τ = 35 h	5840	4869	43
$T_{\text{isothermal}}$ = 25 °C, τ = 35 h	5572	5088	43

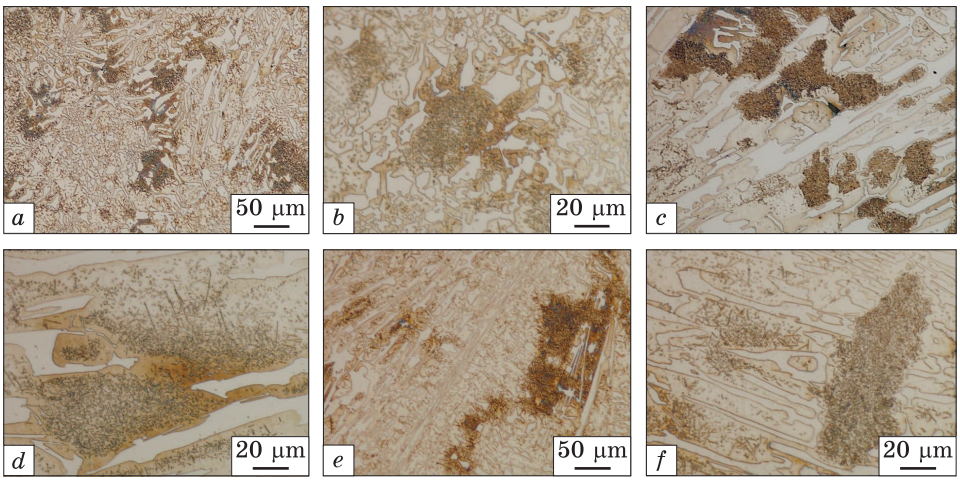

Fig. 27. Microstructure of Cr–Mn–Ni (alloy No. 3) after isothermal soakings at 400–300 °C: T = 400 °C, τ = 40 h (*a*, *b*); T = 350 °C, τ = 35 h (*c*, *d*); T = 300 °C, τ = 40 h (*e*, *f*). Zoom factors: ×200 (*a*, *c*, *e*) and ×500 (*b*, *d*, *f*)

course of curves, with only a slight displacement of transformation start at 300 °C towards the zone of greater austenite resistance.

After isothermal soakings at 300 °C and 200 °C, the ratio of non-decomposed austenite in the structure is 75% and 70%, respectively. At 350 °C, the curve indicates a minimal change in length. After isothermal soaking at 350 °C, the ratio of non-decomposed austenite in the structure is 70%.

The lowest resistance of the initial austenite characterizes the isothermal decomposition pattern of supercooled austenite in alloy No. 3 (Fig. 20), so, the first traces of phase transformations are observed at 350 °C; austenite decomposition begins after 13 h and ends after 21 h.

Figure 27 shows microstructure of chromium–manganese–nickel alloy No. 3 after isothermal soakings in the temperature range of 400–300 °C. After isothermal soaking at 400 °C, the structure exhibits decomposition of supercooled austenite. Probably, the first bainite aggregates appear at the boundary of dendrite and carbide eutectic; these aggregated develop deep into dendrite and carbide eutectic; accumulations of secondary carbides at the boundaries of dendrite and carbide eutectic indicate beginning of formation of bainite aggregates in the initial austenite dendrites.

After isothermal soaking at a temperature of 300 °C, the minimal stability of austenite in the bainite temperature range is observed. Decomposition starts already after 13 h of soaking and is over after 21 h. Decomposition of supercooled austenite occurs with probable formation of bainite aggregates that grow deep into the centre of dendrite. Amount

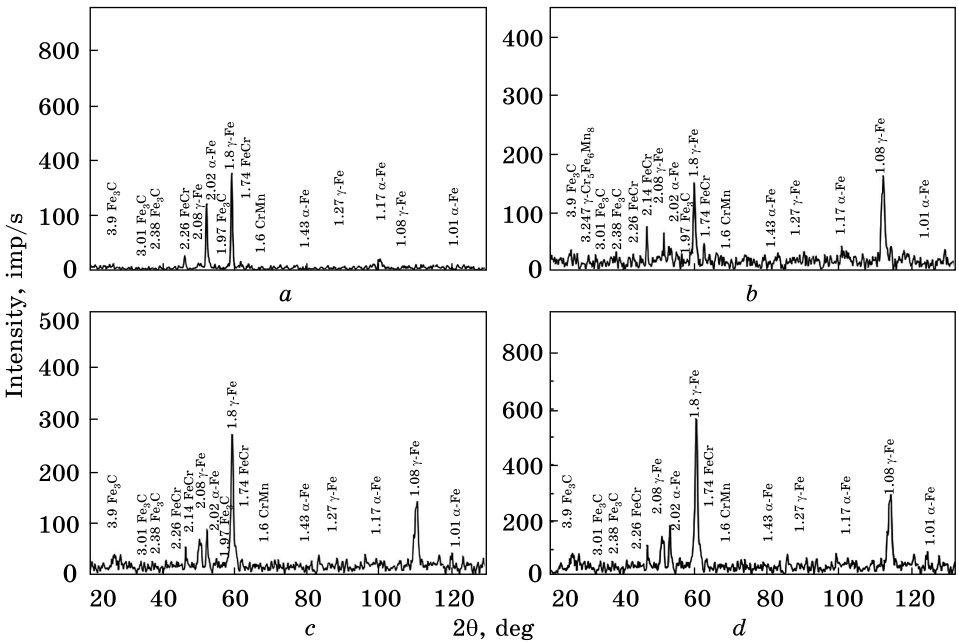

Fig. 28. Diffractograms of Cr–Mn–Ni (alloy No. 3) for isothermal soakings at 400–300 °C: T = 400 °C (*a*); T = 350 °C (*b*); T = 300 °C (*c*); T = 200 °C (*d*)

of decomposed austenite is 25%. After soaking at 200 °C, decomposition of supercooled austenite begins within 17.5 h and finishes within 24 h. Amount of residual austenite in the structure is ≈70%.

Using the x-ray diffraction analysis (Fig. 28), it was determined that the structure of the tested alloy after soaking in the bainite temperature range consists of Me_7C_3 eutectic carbides, austenite decomposition products, Me_7C_3, Me_3C secondary carbides (in all cases, Me = Cr, Mn, Fe) as well as of various amounts of residual austenite.

Thus, the obtained data concerning patterns of structure formation and decomposition kinetics of supercooled austenite in test Cr–Mn–Ni alloys are the basic data for further development of heat processing rational regimes for different kinds of rolling tools.

6. Calorimetric Analysis of Cr–Mn–Ni Alloys

Phase transformations in metal systems are accompanied with a heat release or absorption; sometimes it occurs in the forward and reverse directions (inverted), and sometimes, in one direction (non-inverted) only. The first case includes the following transformations: melting–crystallization, polymorphic transformations, formation–decomposition of chemical compounds. Non-inverted processes include the transformation from low-resistant, metastable compounds to resistant (stable) ones,

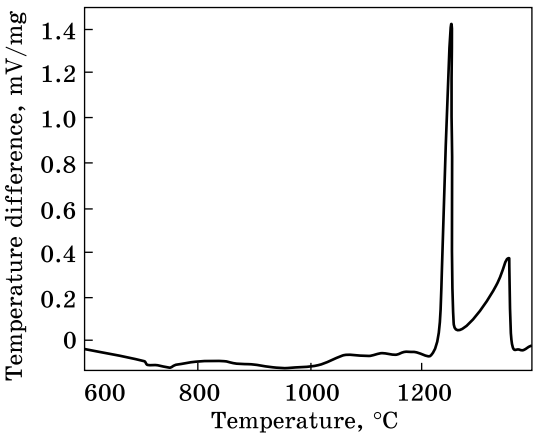

Fig. 29. Heating thermogram of the Cr–Mn–Ni (alloy No. 1)

such as the decomposition of solid solutions, the transition from an amorphous state to a crystalline state. Thermal effects of non-reversed processes are reflected only on the heating curves and, as a rule, such reactions are exothermic.

If in the heating process, the sample does not undergo any transformation, the differential record on the thermogram is fixed as a straight line, parallel to the temperature axis. Thermal effects of phase transformations are reflected in the thermogram by sharp deviations of the differential curve. However, the onset of the effect is characterized by a sharp break on the differential curve only for substances with high thermal conductivity. For materials with a low thermal conductivity, the onset of differential curve deviation is al-ways more or less smoothly rounded.

The temperatures when transformation begins and finishes correspond to the changes of the curve shape. As a rule, the nature of the effect can be determined according to the nature of peaks on the thermogram. However, it should be stressed that currently there is a large number of published thermograms of different materials with unclear effects. An overlap of effects on each other is one of the factors complicating deciphering of thermograms. For instance, if both merging effects are accompanied by heat absorption, then, the thermogram shows one commonly large effect. If two thermal effects (opposite in their sign) merge, then, at an overlapping, they mutually reduce the size of the corresponding deviations on the differential curve. Overlapped peaks of different effects can be deciphered after further studies (tests) using other methods.

In view of the above, let us consider thermograms of chromium–manganese–nickel alloys. Figures 29 and 30 show thermograms of tested alloys. Temperature intervals of phase transformations were determined by the method of thermal analysis using calorimeter at the Physicotechnological Institute of Metals and Alloys of the NAS of Ukraine (Kyiv). The curves are similar in their character with just insignificant shifts of important temperature intervals, which is probably due to the different Mn content in the alloy structures: 5–15% of Mn. The graph shows that, during heating to a temperature of 1150 °C, the thermogram represented by a low-angle line indicates an absence of phase

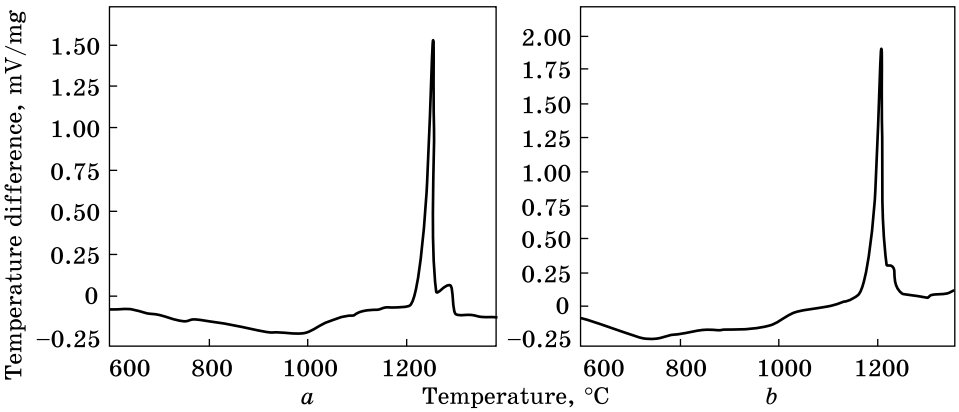

Fig. 30. Heating thermograms of Cr–Mn–Ni alloys: Nos. 2 (*a*) and 3 (*b*)

Table 16. **Liquidus temperatures, solidus temperatures, and eutectic temperatures of the tested alloys**

Tested alloy	Liquidus temperature, °C		Solidus temperature, °C		Eutectic temperature, °C	
	heating	cooling	heating	cooling	heating	cooling
alloy No. 1	1250	1238	1210	1205	1231	1233
alloy No. 2	1246	1230	1185	1190	1224	1226
alloy No. 3	1228	1221	1174	1186	1210	1212

transformations, or these transformations have an insignificant thermal effect.

At this stage, the effects of coagulation and spheroidization of carbides can be overlapped; $\alpha \rightarrow \gamma$ transformation is possible as well as dissociation and dissolution of carbides in austenite. Subsequent heating to the temperatures over 1230–1250 °C leads to melting of the structural components in the tested alloys.

Table 16 shows temperatures of the crystallization onset and melting temperatures for chromium–manganese–nickel alloys, which were determined by the thermal analysis method during the heating and cooling.

7. Tribotechnical Characteristics of Cr–Mn–Ni in the As-Cast State: Influence of Structural–Phase and Stress–Strain States, Physicochemical and Mechanical Properties

This section deals with tests, which we carried out for friction wear at high temperatures and loads as well as for abrasive wear resistance of the chromium–manganese–nickel alloys in the initial as-cast state.

Table 17. **Results of tests on wear resistance for Cr–Mn–Ni alloys in the as-cast state [92]**

No.	Linear wear, μm		Volumetric wear, cm^3		Wear intensity i		Wear resistance coefficient n	
	500 N	600 N	500 N	600 N	500 N	600 N	500 N	600 N
Alloy No. 1								
1	628	568	0.05092	0.12705	$2.33 \cdot 10^{-7}$	$5.81 \cdot 10^{-7}$	6.63	6.24
2	682	622	0.05529	0.05042	$2.53 \cdot 10^{-7}$	$2.31 \cdot 10^{-7}$	6.59	6.63
3	299	145	0.02429	0.11631	$1.11 \cdot 10^{-7}$	$5.32 \cdot 10^{-7}$	6.95	6.27
4	327	232	0.026562	0.03502	$1.22 \cdot 10^{-7}$	$1.60 \cdot 10^{-7}$	6.91	6.79
5	321	118	0.02606	0.08946	$1.19 \cdot 10^{-7}$	$4.09 \cdot 10^{-7}$	6.92	6.39
6	296	218	0.02398	0.12589	$1.10 \cdot 10^{-7}$	$5.76 \cdot 10^{-7}$	6.95	6.24
Alloy No. 2								
7	178	164	0.01445	0.01329	$6.61 \cdot 10^{-8}$	$6.08 \cdot 10^{-8}$	7.17	7.22
8	216	281	0.01756	0.02276	$8.03 \cdot 10^{-8}$	$1.04 \cdot 10^{-8}$	7.09	6.98
9	203	137	0.01645	0.01116	$7.52 \cdot 10^{-8}$	$5.11 \cdot 10^{-8}$	7.12	7.29
10	257	178	0.02086	0.01445	$9.54 \cdot 10^{-8}$	$6.61 \cdot 10^{-8}$	7.02	7.18
11	253	145	0.02051	0.01177	$9.38 \cdot 10^{-8}$	$5.38 \cdot 10^{-8}$	7.02	7.27
12	248	231	0.02009	0.01871	$9.19 \cdot 10^{-8}$	$8.56 \cdot 10^{-8}$	7.03	7.08
Alloy No. 3								
13	153	110	0.01247	0.00894	$5.70 \cdot 10^{-8}$	$4.09 \cdot 10^{-8}$	7.24	7.34
14	169	152	0.01373	0.01232	$6.20 \cdot 10^{-8}$	$5.64 \cdot 10^{-8}$	7.20	7.25
15	175	212	0.01424	0.01718	$6.51 \cdot 10^{-8}$	$7.86 \cdot 10^{-8}$	7.18	7.11
16	165	166	0.01336	0.01346	$6.11 \cdot 10^{-8}$	$6.16 \cdot 10^{-8}$	7.21	7.21
17	220	196	0.01782	0.01594	$8.15 \cdot 10^{-8}$	$7.29 \cdot 10^{-8}$	7.08	7.14
18	163	155	0.01323	0.01768	$6.05 \cdot 10^{-8}$	$8.09 \cdot 10^{-8}$	7.21	7.09

Table 18. **Results of the abrasive wear resistance testing of Cr–Mn–Ni [82]**

Abrasive	Time, min	Wear of alloys, mg		
		alloy No. 1	alloy No. 2	alloy No. 3
Sand	15	2.7	3.5	1
	20	2.9	4.5	2.4
	25	3.4	6.7	3
Boron carbide	15	20.1	25.9	28.8
	20	31.5	32.6	29.5
	25	49	47.1	34.8
Silicon carbide	15	33	35.4	30.5
	20	42.6	39.3	46.3
	25	51	53.2	50

Results of the tests for friction wear of the Cr–Mn–Ni alloys in the as-cast state are presented in Table 17 and Fig. 31. Analysis of the data indicates that alloy No. 3 is characterized by the highest wear resistance (minimum wear intensity and high wear resistance coefficient) in the result of friction wear at elevated temperatures. High wear resistance of this alloy is associated with a high microhardness of its matrix, austenite–carbide eutectics based on Me_7C_3 carbide; and it is determined by the alloying degree, shape parameter of the eutectic carbide, and the deformation-induced phase transformations occurring in the alloys at the friction wear process.

Table 18 shows results of testing the alloys for abrasion resistance, and Figs. 32–34 show the wear diagrams of chromium–manganese–nickel alloys. Analysis of the data presented in Table 18 and Figs. 32–34 indicates that at the initial stage of testing (wear time of 15 minutes), the mass loss for all tested alloys is minimal, and with the increase of the test time up to 25 minutes, the mass loss increases in all cases. The maximal mass loss in the process of testing under conditions of an abrasive environment (silicon oxide) is observed in case with alloy No. 2, and the minimal mass loss is typical for alloy No. 3. In the process of performing tests under conditions of an abrasive environment (boron carbide), the maximal mass loss was observed in alloy No. 1, and the minimal mass loss was typical for alloy No. 3. In the process of testing under conditions of an abrasive environment (silicon carbide), the maximal loss was observed in alloy No. 2, and the minimal mass loss was typical for alloy No. 3.

Thus, the performed analysis of the obtained data shows that alloy No. 3 possesses the highest abrasive wear resistance at the conditions of different abrasive environments. High abrasive wear resistance of this alloy is associated with a high microhardness of its matrix, Me_7C_3-carbide-based austenite–carbide eutectics, and it is determined by the degree of alloying and shape parameter of the eutectic carbide, as well as by deformation-induced phase transformations occurring in the tested alloys in the process of abrasive wear.

8. Conclusions

The structure, phase composition, and properties of Cr–Mn–Ni alloys (12–16% of Cr, 6–15% of Mn, and 0.8–1.5% of Ni) in the initial as-cast state are studied. Such alloys are used for manufacturing parts of rolling tools of metallurgical equipment (rolling mills, rulers and rolling mill frameworks). Microstructure of tested alloys includes Me_7C_3 carbides (both in the longitudinal and transverse sections) and fine-differentiated Me_7C_3 carbide-based austenite–carbide eutectics. Obtained results enable us to conclude as follow.

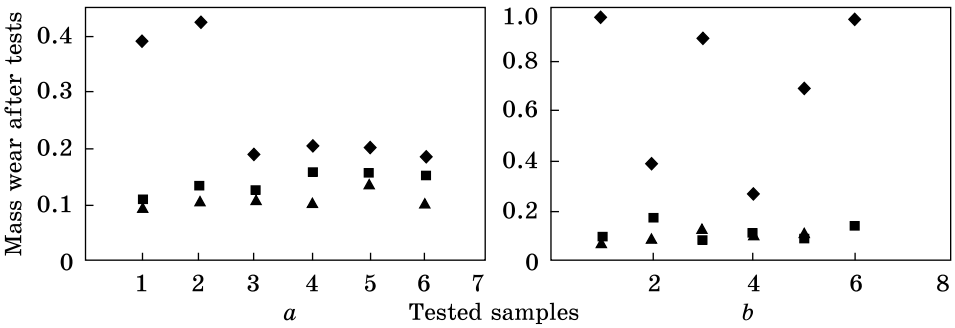

Fig. 31. Mass wear of Cr–Mn–Ni alloys in the as-cast state as a result of friction wear tests at the loads of 500 N (*a*) and 600 N (*b*), where diamonds (♦), squares (■), and triangles (▲) correspond to alloys Nos. 1, 2, and 3, respectively [92]

Fig. 32. Mass loss of the Cr–Mn–Ni alloys in the as-cast state in the process of testing in conditions of an abrasive environment (silicon oxide), where diamonds (♦), squares (■), and triangles (▲) correspond to alloys Nos. 1, 2, and 3, respectively [82]

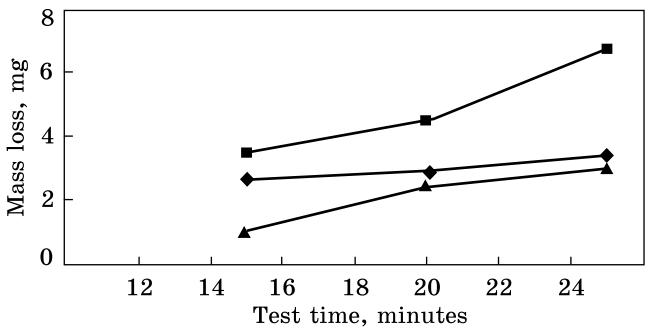

Fig. 33. The same as in the previous figure, but for another abrasive agent, namely, boron carbide, where diamonds (♦), squares (■), and triangles (▲) correspond to alloys Nos. 1, 2, and 3, respectively [75]

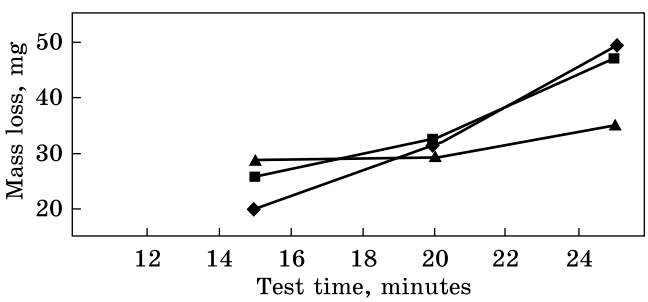

Fig. 34. The same as in Fig. 32, but for another abrasive agent, namely, silicon carbide, where diamonds (♦), squares (■), and triangles (▲) correspond to alloys Nos. 1, 2, and 3, respectively [82]

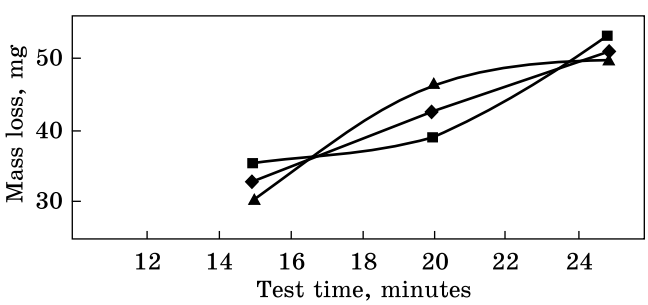

• The quantitative ratio of initial austenite dendrites and eutectic component is determined by the carbon content and the ratio of the main alloying elements (Cr and Mn).

• The hardness of the Cr–Mn–Ni alloys is determined by the C and Mn contents as well as by the amount of the carbide component.

• The maximal strength and hardness in the as-cast state are typical for alloys Nos. 2–3; this gives an opportunity to predict the increase of abrasive wear resistance and impact-abrasive wear resistance in the as-cast and heat-treated states.

• Amount of austenite in the matrix of the tested alloys grows from 87% to 94% with increase of C content and content of alloying elements (Cr and Mn); and amount of ferrite decreases, respectively, from 13% to 6% (Table 4).

• Distribution of alloying elements between the phases and structural components in the Cr–Mn–Ni alloys is investigated. By means of the local x-ray spectral analysis it was determined that in the tested alloys in eutectic carbide chromium is present in quantities of ≈34.9–36.7%, amount of Mn is 8.9–9.33%, and percentage of Si is 0.11–0.23%. Results of local x-ray spectral analysis of distribution of alloying elements between phases and structural components indicate that with increase of C, Cr, and Mn in the tested alloys, the degree of alloying the matrix and eutectic carbide increases, which ensures increased microhardness, hardness, and, respectively, improved wear resistance.

• Kinetics of bainitic transformation and regularities of bainitic nanostructured matrix formation in the Cr–Mn–Ni alloys are investigated. Diagrams of isothermal transformation of austenite in the tested alloys are obtained.

• Phase transformations of Cr–Mn–Ni alloys are studied using a high-temperature differential thermal analyser. Liquidus and solidus temperatures are determined.

• Tribological properties of as-cast Cr–Mn–Ni alloys are investigated. Regularities of influence of physicochemical and mechanical properties (caused by the structural–phase and stress–strained states) as well as dispersibility of matrix components on tribotechnical characteristics of these alloys are determined.

• Maximal values of wear resistance and minimal values of wear intensity under conditions of different abrasive environments as well as under conditions of friction at high loads and temperatures are typical for the Cr–Mn–Ni alloy with Cr content of 13%, Mn content of 15%, and Ni content of 1.2% (alloy No. 3).

REFERENCES

1. V.Z. Kutsova, M.A. Kovzel, P.U. Shvets, A.V. Grebeneva, and V.V. Prutchykova, *Metallofiz. Noveishie Tekhnol.*, **40**, No. 4: 551 (2018). https://doi.org/10.15407/mfint.40.04.0551
2. O.I. Soshko and V.O. Soshko, *Prog. Phys. Met.*, **20**, No. 1: 96 (2019). https://doi.org/10.15407/ufm.20.01.096
3. A.I. Stepina, A.M. Stupitsky, and I.R. Klais, *Liteinoye Proizvodstvo*, No. 9: 26 (1977) (in Russian).
4. A.D. Leshchenko, A.D. Kutuzov, and V.V. Lunev, *Liteinoye Proizvodstvo*, No. 6: 8 (1988) (in Russian).
5. O.S. Komarov, O.A. Susina, and N.I. Urbnovich, *Litye i Metallurgiya. Inf. Byulleten*, Nos. 7–9: 22 (1997) (in Russian).
6. M.P. Shebatnov, L.I. Romanov, M.I. Prokhorov, and E.V. Boldyrev, *Trudy Gorkovskogo Instituta Vodnogo Transporta*, 1984, No. 206: 99 (1984) (in Russian).
7. I.N. Slabodinsky, B.A. Kirievsky, and L.G. Smolyakov, *Litye i Iznosostoikie Materialy: Sbornik IPL AN USSR* (Kiev: Institut Problem Lit'ya: 1972), p. 21 (in Russian).
8. G.V. Samsonov and I.M. Vinnitskiy, *Tugoplavkie Soedineniya* [Refractory Compounds] (Moscow: Metallurgiya: 1976) (in Russian).
9. E. Houdremont, *Spetsialnyye Stali* [Special Steels] (Moscow: Metallurgiya: 1959) (Russian translation).
10. V.S. Popov, N.N. Brykov, N.S. Dmitrichenko, and P.G. Fit, *Dolgovechnost Oborudovaniya Ogneupornogo Proizvodstva* [The Durability of the Equipment of Refractory Production] (Moscow: Metallurgiya: 1977) (in Russian).
11. Yu.G. Bobro, *Legirovannyye Chuguny* [Alloyed Cast Irons] (Moscow: Metallurgiya: 1976) (in Russian).
12. K.P. Bunin and Yu.N. Taran, *Stroenie Chuguna* [The Structure of Cast Iron] (Moscow: Metallurgiya: 1972) (in Russian).
13. V.I. Nikitin, *Raschet Zharostoikosti Metallov* [Calculation of the Heat Resistance of Metals] (Moscow: Metallurgiya: 1976) (in Russian).
14. N.I. Bestuzhev and S.P. Korolev, *Liteinoye Proizvodstvo*, No. 3: 20 (1999) (in Russian).
15. V.M. Sadovsky, O.S. Komarov, and S.N. Herzik, *Liteinoye Proizvodstvo*, No. 5: 12 (1998) (in Russian).
16. R. Hosen, E.Kh. Ri, and V.A. Teich, *Liteinoye Proizvodstvo*, No. 10: 15 (2000).
17. V.P. Gavrilyuk, E.A. Markovsky, and L.I. Butenko, *Liteinoye Proizvodstvo*, No. 7: 20 (1998) (in Russian).
18. L.G. Savina, E.E. Baryshev, and M.A. Filipov, *Teoriya i Praktika Metallurgii*, Nos. 4–5: 121 (2006) (in Russian).
19. K.P. Bunin, Y.N. Malinochka, and Y.N. Ram, *Osnovy Metallografii Chuguna* [Fundamentals of Cast Iron Metallography] (Moscow: Metallurgiya: 1969) (in Russian).
20. I.I. Tsypin, *Belyye Iznosostoikie Chuguny* [White Wear-Resistant Cast Irons] (Moscow: Metallurgiya: 1983) (in Russian).
21. *Friction, Wear, and Lubrication: Guide* (Eds. I.V. Kragelsky and V.V Alisin) (Pergamon: 1982).
22. M.M. Tenenbaum, *Iznosostoykost Konstruktsionnykh Materialov i Detaley Mashin* [Wear Resistance of Structural Materials and Machine Parts] (Moscow: Mashinostroenie: 1966) (in Russian).

23. V.I. Tikhnovich, V.P. Gavrilyuk, and I.A. Shalevskaya, *Protsessy Litya*, No. 2: 84 (2005) (in Russian).
24. V.N. Kashcheev, *Abrazivnoye Razrushenie Tverdykh Tel* [Abrasive Destruction of Solids] (Moscow: Nauka: 1970 (in Russian).
25. I.V. Kragelsky, *Trenie i Iznos* [Friction and Wear] (Moscow: Mashinostroenie: 1968) (in Russian).
26. E.V. Rozhkova, O.M. Romanov, L.Ya. Kozlov, and L.M. Romanov, *Metallovedenie i Termicheskaya Obrabotka Metallov*, No. 6: 30 (1986) (in Russian).
27. V.I. Tikhonovich, O.I. Kovalenko, and V.A. Loktionov, *Litye Iznosostoikie Materialy, Ikh Razrabotka i Primenenie* [Cast Wear-Resistant Materials, Their Development and Application] (Kiev: Znanie: 1980) (in Russian).
28. A.N. Poddubny, *Liteinoye Proizvodstvo*, No. 3: 7 (1997) (in Russian).
29. V.P. Grechin, *Iznosostoikie Chuguny i Splavy* [Wear-Resistant Cast Irons and Alloys] (Moscow: Mashgiz: 1961) (in Russian).
30. Z.M. Gamolskaya, V.M. Guterman, and N.A. Didkovskaya, *Iznosostoikie Materialy dlya Detaley Gornykh Mashin* [Wear-Resistant Materials for Parts of Mining Machines] (VNIIIPTuglemash. Nedra: 1972), vol. **17**, p. 1 (in Russian).
31. I.E. Lev, *Karbidnyy Analiz Chuguna* [Carbide Analysis of Cast Iron] (Kharkov: Metallurgizdat: 1962) (in Russian).
32. I.N. Slabodinsky, A.F. Sofromenkov, and N.V. Korshikova, *Izvestiya VUZov. Chernaya Metallurgiya*, No. 8: 77 (1980) (in Russian).
33. A.G. Vinnitsky and D.Y. Vishnyakov, *Metallovedenie i Termicheskaya Obrabotka Metallov*, No. 4: 2 (1957) (in Russian).
34. B.I. Kostetsky, *Trenie, Smazka i Iznos v Mashinakh* [Friction, Lubrication and Wear in Machines] (Kiev: Tekhnika: 1970) (in Russian).
35. N.D. Tomashov, *Teoriya Korrozii i Zashchity Metallov* [The Theory of Corrosion and Metal Protection] (Moscow: Metallurgizdat: 1960 (in Russian).
36. *Cast Iron: Handbook* (Eds. A.D. Sherman and A.A. Zhukov) (Moscow: Metallurgiya: 1991) (in Russian).
37. M.A. Fillipov, P. Lhagvadorzh, and G.N. Plotnikov, *Metallovedenie i Termicheskaya Obrabotka Metallov*, No. 11: 10 (2000) (in Russian).
38. K.N. Minyailovskiy, *Fazovyye Prevrashcheniya pri TO Iznosostoikikh Vysokokhromistykh Chugunov* [Phase Transformations during Maintenance of Wear-Resistant of High-Chromium Cast Irons] (Diss. for Cand. Tech. Sci.) (Alchevsk: Kommunarsk Mining and Smelting Institute: 1969) (in Russian).
39. M.M. Khrushchov and M.A. Babichev, *Abrazivnoe Iznashivanie* [Abrasive Wear] (Moscow: Nauka: 1970) (in Russian).
40. M.M. Tenenbaum, *Soprotivlenie Abrazivnomu Iznashivaniyu* [Resistance to Abrasive Wear] (Moscow: Mashinostroenie: 1976) (in Russian).
41. F.P. Bowden and D. Teibor, *Trenie i Smazka Tverdykh Tel* [Friction and Lubrication of Solids] (Moscow: Mashinostroenie: 1968) (in Russian).
42. N.I. Bogomolov, *Metody Ispytaniya na Iznashivanie* [Methods of Wear Tests] (Moscow: Izdatelstvo AN SSSR: 1962), p. 12 (in Russian).
43. T.S. Skoblo, E.G. Popova, N.A. Budagyants, and N.A. Zhizhkina, *Liteinoye Proizvodstvo*, No. 8: 7 (2001) (in Russian).
44. A.N. Poddubniy, I.K. Kulbovskiy, and A.V. Dyukov, *Liteinoye Proizvodstvo*, No. 5: 46 (1997) (in Russian).
45. V.Z. Somin, A.D. Andreev, and V.I. Kulikov, *Liteinoye Proizvodstvo*, 2002. No. 11: 16 (2002) (in Russian).
46. V.A. Voinov, *Iznosostoikie Splavy i Pokrytiya* [Wear-Resistant Alloys and Coatings] (Moscow: Mashinostroenie: 1980) (in Russian).

47. M.E. Garber, *Otlivki iz Belykh Iznosostoikikh Chugunov* [Castings from White Wear-Resistant Cast Irons] (Moscow: Mashinostroenie: 1972) (in Russian).
48. A.A. Kosilov, A.A. Kruglov, and V.N. Rebonen, *Liteinoye Proizvodstvo*, No. 6: 13 (2001) (in Russian).
49. B.I. Voronenko, *Liteinoye Proizvodstvo*, No. 10: 8 (1993) (in Russian).
50. O.G. Sokolov and K.B. Katzov, *Zhelezomargantsevyye Splavy* [Ferromanganese Alloys] (Kiev: Naukova Dumka: 1982) (in Russian).
51. *GOST 977-88. Otlivki Stalnye. Obshchie Tekhnicheskiye Usloviya* [Steel Castings. General Specifications] (Moscow: Izdatelstvo Standartov: 1989) (in Russian).
52. W. Jellinghaus and H. Keller, *Archiv fur das Eisenhuttenwesen*, **43**, No. 3: 193 (1972) (in German).
53. I.N. Bogachev and R.I. Mintz, *Kavitatsionnoye Razrushenie Zhelezouglerodistykh Splavov* [Cavitational Destruction of Iron–Carbon Alloys] (Moscow: Mashgiz: 1959) (in Russian).
54. M.A. Fillipov, V.S. Litvinov, and Yu.R. Nemirovsky, *Stali s Metastabilnym Austenitom* [Steel with Metastable Austenite] (Moscow: Metallurgiya: 1988) (in Russian).
55. L.S. Malinov and V.L. Malinov, *Metallurgical and Mining Industry*, No. 6: 39 (1999) (in Russian).
56. V.S. Popov, N.N. Brykov, and N.S. Dmitrichenko *Iznosostoykost Pressform Ogneupornogo Proizvodstva* [Wear Resistance of Moulds of Refractory Production] (Moscow: Metallurgiya: 1971) (in Russian).
57. G.I. Silman and N.V. Dmitrieva, *Materialovedenie i Proizvodstvo: Mezhvuzovskiy Sbornik Nauchnykh Trudov* (Izdatelstvo BGITA), **2**: 241 (2001) (in Russian).
58. A.P. Cheylyakh, I.M. Oleinik, and E.B. Lokshina, *Metals*, No. 1: 66 (2001) (in Russian).
59. A.P. Cheylyakh, D.V. Klok, and S.V. Fine, *Metal and Casting of Ukraine*, Nos. 9–10: 13 (2006) (in Russian).
60. T.M. Mironova, P.F. Nizhnikovskaya, and Yu.N. Taran, *Voprosy Formirovaniya Metastabilnykh Struktur Splavov: Mezhvuzovskiy Sbornik Nauchnykh Trudov* (Dnepropetrovsk: Izdatelstvo DGU: 1981), p. 132 (in Russian).
61. G.I. Silman, *Metallovedenie i Termicheskaya Obrabotka Metallov*, No. 9: 3 (2005) (in Russian).
62. O.M. Khoroshylov, V.V. Kurylyak, O.S. Podolyak, and N.S. Antonenko, *Prog. Phys. Met.*, **20**, No. 3: 367 (2019). https://doi.org/10.15407/ufm.20.03.367
63. P. Puspitasari and J.W. Dika, *Prog. Phys. Met.*, **20**, No. 3: 396 (2019). https://doi.org/10.15407/ufm.20.03.396
64. H.T. Angus, *Cast Iron: Physical and Engineering Properties* (London: Butterworth-Heinemann: 1976). https://doi.org/10.1016/C2013-0-01035-3
65. M.A. Fesenko and A.M. Fesenko, *Prog. Phys. Met.*, **21**, No. 1: 83 (2020). https://doi.org/10.15407/ufm.21.01.83
66. V.B. Molodkin, H.I. Nizkova, Ye.I. Bogdanov, S.I. Olikhovskii, S.V. Dmitriev, M.G. Tolmachev, V.V. Lizunov, Ya.V. Vasylyk, A.G. Karpov, and O.G. Voytok, *Usp. Fiz. Met.*, **18**, No. 2: 177 (2017) (in Ukrainian). https://doi.org/10.15407/ufm.18.02.177
67. V.V. Lizunov, I.M. Zabolotnyy, Ya.V. Vasylyk, I.E. Golentus, and M.V. Ushakov, *Prog. Phys. Met.*, **20**, No. 1: 75 (2019). https://doi.org/10.15407/ufm.20.01.075

68. T.M. Radchenko, V.A. Tatarenko, V.V. Lizunov, V.B. Molodkin, I.E. Golentus, I.Yu. Sahalianov, and Yu.I. Prylutskyy, *Phys. Status Solidi B*, **256**, No. 5: 1800406 (2019).
https://doi.org/10.1002/pssb.201800406
69. V.Z. Kutsova, M.A. Kovzel, A.V. Grebeneva, I.V. Ratnikova, and O.O. Velichko, *Metallurgical and Mining Industry*, No. 9: 1084 (2015).
70. S.A. Saltykov, *Stereometricheskaya Metallografiya* [Stereometric Metallography] (Moscow: Metallurgy: 1970) (in Russian).
71. F.R. Wilson and R.A. Harding, *BCIRA Report No. 1783* (Birmingham, UK: 1989).
72. L.I. Mirkin, *Rentgenostrukturnyy Kontrol Mashinostroitelnykh Materialov* [X-Ray Control of Engineering Materials] (Moscow: Mashinostroenie: 1979) (in Russian).
73. S.S. Gorelik, A.N. Rastorguev, and Yu.A. Skakov, *Rentgenograficheskiy i Ehlektronno-Graficheskiy Analiz Metallov* [X-Ray and Electron Diffraction Analysis of Metals] (Moscow: Metallurgy: 1963) (in Russian).
74. M.A. Tylkin, *Spravochnik Termista Remontnoy Sluzhby* [The Handbook of the Heat-Treater of the Repair Service] (Moscow: Metallurgiya: 1981) (in Russian).
75. G.V. Samsonov, T.Ya. Kosolapova, and V.S. Neshpor, *Karbidy i Splavy na Ikh Osnove* [Carbides and Their-Based Alloys] (Kiev: Naukova Dumka: 1976) (in Russian).
76. E.P. Kalinushkin, *Peritekticheskaya Kristallizatsiya Legirovannykh Splavov na Osnove Zheleza* [Peritectic Crystallization of Iron-Based Doped Alloys] (Dnepropetrovsk: Porogi: 2007); K. Niihara, *J. Mater. Sci. Lett.*, **2**: 221 (1983).
https://doi.org/10.1007/BF00725625
77. N.V. Novikov, S.N. Oak, and S.I. Bulychov, *Zavodskaya Laboratoriya*, No. 7: 60 (1988) (in Russian).
78. V.I. Dvoruk and M.V. Matrosov, *Problems of Friction and Wear*, No. 50: 44 (2008) (in Ukrainian).
https://doi.org/10.18372/0370-2197.50.2946
79. M.V. Kindrachuk, E.A. Kulgavyy, O.L. Shevchenko, and A.P. Danilov, *Naukoyemni Tekhnologii*, **1**, No. 1: 102 (2009) (in Ukrainian).
https://doi.org/10.18372/2310-5461.1.5205
80. M.I. Denysenko, V.F. Labunets, and V.V. Zahrebelnyi, *Problems of Friction and Wear*, No. 1 (66): 113 (in Ukrainian).
https://doi.org/10.18372/0370-2197.1(66).9361
81. V.Z. Kutsova, M.V. Kindrachuk, M.A. Kovzel, O.V. Tisov, A.V. Grebeneva, and P.Y. Shvets, *Problems of Friction and Wear*, No. 2 (71): 78 (2016) (in Ukrainian).
https://doi.org/10.18372/0370-2197.2(71).11069
82. Yu.N. Taran, V.Z. Kutsova, A.Yu. Kutsov, and M.A. Kovzel, *Stroitelstvo, Materialovedenie, Mashinostrenie*, **27**, part 1: 38 (2004) (in Russian).
83. H.K.D.H. Bhadeshia and J.W. Christian, *Metall. Trans. A*, **21**: 767 (1990).
https://doi.org/10.1007/BF02656561
84. A.M. Nesterenko, V.Z. Kutsova, and M.A. Kovzel, *Metallofiz. Noveishie Tekhnol.*, No. 1: 99 (2003).
85. V.Z. Kutsova, M.A. Kovzel, A.V. Grebeneva, I.V. Ratnikova, and P.Y. Shvets, *Stroitelstvo, Materialovedenie, Mashinostroenie: Sbornik 'Starodubovskie Chteniya'*, No. 89: 101 (2016) (in Russian).
86. V.Z. Kutsova, M.A. Kovzel, A.V. Grebeneva, P.Y. Shvets, A. Zyska, and B. Koczurkiewicz, *Proc. XIX Int. Sci. Conf. 'New Technologies and Achievements in Metallurgy, Material Engineering and Production Engineering and Physics'. A Collective Monograph. Series: Monograph, No. 78* (Częstochowa: Częstochowa University of Technology: 2018), p. 147.

87. V.Z. Kutzova, M.A. Kovzel, and A.V. Grebeneva, *Metaloznavstvo ta Obrobka Metaliv*, No. 2: 43 (2017) (in Ukrainian).
88. M. Hillert, *ISIJ Intern.*, **35**, No. 9: 1134 (1995). https://doi.org/10.2355/isijinternational.35.1134
89. V.Z. Kutsova, A.Yu. Kutsov, and M.A. Kovzel, *Proc. of Forum 'Education–Investments–Research & Development (July 4–10, 2006, Davos)*, p. 82.
90. L.G. Berg, *Vvedenie v Termografiyu* [Introduction to Thermography] (Moscow: Izd. Akad. Nauk SSSR: 1961), p. 56 (in Russian).
91. G.O. Piloyan, *Vvedenie v Teoriyu Termicheskogo Analiza* [Introduction to the Theory of Thermal Analysis] (Moscow: Izd. Akad. Nauk SSSR: 1984) (in Russian).
92. V.Z. Kutsova, M.A. Kovzel, A.V. Grebeneva, P.Y. Shvets, A. Zyska, and Z. Konopka, *Proc. XVIII Int. Conf. 'New Technologies and Achievements in Metallurgy, Material Engineering and Production Engineering and Physics'. A Collective Monograph. Series: Monograph, No. 68* (Częstochowa: Częstochowa University of Technology: 2017), p. 53.

Received 10.01.2020;
in final version, 12.05.2020

Ю.М. Коваль[1], *В.З. Куцова*[2], *М.А. Ковзель*[2], *П.Ю. Швець*[2]

[1] Інститут металофізики ім. Г.В. Курдюмова НАН України,
бульв. Академіка Вернадського, 36,
03142 Київ, Україна

[2] Національна металургійна академія України,
пр. Гагаріна, 4, 49000 Дніпро, Україна

ОСОБЛИВОСТІ СТРУКТУРОУТВОРЕННЯ, КІНЕТИКИ ФАЗОВИХ ПЕРЕТВОРЕНЬ, МЕХАНІЧНИХ І ТРИБОЛОГІЧНИХ ВЛАСТИВОСТЕЙ СТОПІВ Cr–Mn–Ni НА ОСНОВІ Fe

У роботі оглянуто та проаналізовано вирішення науково-практичної задачі, яка полягає у підвищенні комплексу трибологічних властивостей і жароміцности стопів на основі заліза для сучасного машинобудування. Розроблено склад нових економнолегованих зносостійких хромоманганонікелевих стопів на основі заліза. Вивчено розподіл легувальних елементів між фазами та структурними складовими, встановлено залежність зміни механічних властивостей від параметрів структури та фазового складу. Вперше методом дилатометрії досліджено кінетику бейнітного перетворення та закономірності формування наноструктурної бейнітної матриці стопів Cr–Mn–Ni на основі Fe. Побудовано діаграми ізотермічного розпаду переохолодженого аустеніту. Досліджено трибологічні властивості Cr–Mn–Ni-стопів у литому стані.

Ключові слова: хромоманганонікелеві стопи, структура, зносостійкість, бейніт, абразивне зношування.

Ю.Н. Коваль[1], *В.З. Куцова*[2], *М.А. Ковзель*[2], *П.Ю. Швец*[2]

[1] Институт металлофизики им. Г.В. Курдюмова НАН Украины,
бульв. Академика Вернадского, 36,
03142 Киев, Украина

[2] Национальная металлургическая академия Украины,
пр. Гагарина, 4, 49000 Днепр, Украина

ОСОБЕННОСТИ СТРУКТУРООБРАЗОВАНИЯ, КИНЕТИКИ ФАЗОВЫХ ПРЕВРАЩЕНИЙ, МЕХАНИЧЕСКИХ И ТРИБОЛОГИЧЕСКИХ СВОЙСТВ СПЛАВОВ Cr–Mn–Ni НА ОСНОВЕ Fe

В работе обозреваются и анализируются решения научно-практической задачи, которая заключается в повышении комплекса трибологических свойств и жаропрочности сплавов на основе железа для современного машиностроения. Разработан состав новых экономнолегированных износостойких хромомарганцевоникелевых сплавов на основе железа. Изучено распределение легирующих элементов между фазами и структурными составляющими, установлена зависимость изменения механических свойств от параметров структуры и фазового состава. Впервые методом дилатометрии исследована кинетика бейнитного превращения и закономерности формирования наноструктурной бейнитной матрицы сплавов Cr–Mn–Ni на основе Fe. Построены диаграммы изотермического распада переохлаждённого аустенита. Исследованы трибологические свойства Cr–Mn–Ni-сплавов в литом состоянии.

Ключевые слова: хромомарганцевоникелевые сплавы, структура, износостойкость, бейнит, абразивный износ.